DESIGN OF FRACTAL ANTENNAS FOR RFID AND WIRELESS COMMUNICATION

ECMEL MEHMET CETER

ÖZYEĞİN UNIVERSITY

DECEMBER, 2025

DESIGN OF FRACTAL ANTENNAS FOR RFID AND WIRELESS COMMUNICATION

by
Ecmel Mehmet Ceter

Thesis
Submitted in Partial Fulfillment of the
Requirements for the Degree of

Master of Science

in
Electrical and Electronics Engineering

Advisor: Asst. Prof. Göktürk Poyrazoğlu

Graduate School of Science and Engineering
Özyeğin University
İstanbul

December, 2025

DESIGN OF FRACTAL ANTENNAS FOR RFID AND WIRELESS COMMUNICATION

Approved by:

Asst. Prof. Göktürk Poyrazoğlu, Advisor
Department of Electrical and Electronics Engineering
Özyeğin University

Prof. Dr. Hüseyin Arda Ülkü
Department of Electrical and Electronics Engineering
Yeditepe University

Asst. Prof. Ahmed Akgiray
Department of Electrical and Electronics Engineering
Özyeğin University

Approval Date: November 06, 2025

To my family...

DECLARATION OF ORIGINALITY

I hereby declare that I am the sole author of this thesis and that this is the true copy of my thesis, including the final revisions, approved by my thesis committee. All data and information have been obtained, produced and presented in accordance with the rules of research ethics and principles of academic honesty. As required by these rules, to the best of my knowledge I have acknowledged ideas, thoughts and any copyrighted material in accordance with the standard referencing rules. I certify that any part of this thesis has not been submitted for a degree or diploma in another educational institution.

Ecmel Mehmet Ceter

ABSTRACT

This thesis presents the design, simulation and comparative performance analysis of a multiband fractal antenna based on the third iteration of the Koch curve, intended for Radio Frequency Identification (RFID) and wireless communication systems. The study explores how substrate material properties, particularly dielectric constant and loss tangent, influence antenna performance by implementing the same antenna geometry on two substrates: conventional FR-4 and high permittivity Alumina (Al_2O_3). The antenna structures were modeled and optimized using the ANSYS HFSS (Swanson Analysis Systems High Frequency Structure Simulator), with comprehensive parametric sweeps conducted to evaluate the impact of critical design parameters, including ground plane dimensions, feedline width and patch height. The designs were evaluated in terms of return loss (S_{11}), Voltage Standing Wave Ratio (VSWR), bandwidth, radiation patterns (2D and 3D) and gain across multiple frequency bands. Simulation results indicate that the use of Alumina, with its relative permittivity of $\varepsilon_r \approx 9.8$, enables considerable size reduction of the antenna while maintaining acceptable radiation efficiency and multiband performance. Conversely, the FR-4 based design, with $\varepsilon_r \approx 4.4$, provides broader bandwidth but at the cost of increased physical dimensions. The results further demonstrate that the Alumina based design exhibits sharp resonance characteristics suitable for compact UHF RFID tag or reader integration, whereas the FR-4 design provides wide bandwidth, allowing tolerances to be disregarded during application. The antennas achieved resonant frequencies at approximately 866 MHz, 2.4 GHz and 5.8 GHz, making them suitable for EPC Gen2 RFID, Wi-Fi and industrial wireless applications. The use of a fractal geometry not only enabled size reduction but also facilitated multiband operation due to the self similarity and space filling characteristics inherent in the Koch structure. This work contributes to the field of substrate aware antenna engineering by offering a systematic comparison between low and high permittivity materials in fractal antenna design and provides design guidelines for selecting suitable substrates based on size, frequency and bandwidth requirements.

Keywords: Fractal antennas, koch curve, multiband antenna, alumina, dielectric substrate

ÖZET

Bu tez çalışmasında, üçüncü iterasyon Koch eğrisine dayalı çok bantlı bir fraktal antenin tasarımı, benzetimi ve karşılaştırmalı performans analizi sunulmuştur. Anten, Radyo Frekansı Tanımlama (RFID) ve kablosuz iletişim sistemleri için geliştirilmiş olup, aynı anten geometrisi kullanılarak farklı alttaş malzemelerinin geleneksel FR-4 ve yüksek dielektrik sabitine sahip Alumina (Al_2O_3) anten performansı üzerindeki etkileri incelenmiştir. Anten yapıları, ANSYS HFSS (High Frequency Structure Simulator) yazılımı kullanılarak modellenmiş ve optimize edilmiştir. Toprak düzlemi boyutları, besleme hattı genişliği ve boyu gibi kritik tasarım parametrelerinin etkilerini değerlendirmek amacıyla kapsamlı parametrik analizler gerçekleştirilmiştir. Tasarımlar, geri yansıma katsayısı (S_{11}), Gerilim Duran Dalga Oranı (VSWR), bant genişliği, 2D ve 3D ışıma desenleri ve kazanç parametrelerine göre değerlendirilmiştir. Simülasyon sonuçları, yaklaşık $\varepsilon_r \approx 9.8$ dielektrik sabitine sahip Alumina alttaşının, anten boyutunun önemli ölçüde küçültülmesini sağlarken yeterli düzeyde ışıma verimliliği ve çok bantlı performans sunduğunu göstermektedir. Buna karşılık, $\varepsilon_r \approx 4.4$ olan FR-4 tabanlı tasarım daha geniş bant aralığı sunmakta ancak fiziksel boyut açısından daha büyüktür. Alumina bazlı tasarım, keskin rezonans tepkisi ile UHF RFID etiket/okuyucu uygulamaları için uygunken, FR-4 tasarımı, geniş bant sağlayarak uygulama sırasında toleransları göz ardı etmeye yaramaktadır. Tasarım, yaklaşık olarak 866 MHz, 2.4 GHz ve 5.8 GHz rezonans frekanslarına ulaşmış; bu da RFID, Wi-Fi ve endüstriyel kablosuz uygulamalarla uyum sağlamıştır. Fraktal geometri sayesinde, kendine benzerlik ve alan doldurma özellikleri sayesinde hem çok bantlı çalışma sağlanmış hem de anten boyutu küçültülmüştür. Bu çalışma, düşük ve yüksek dielektrik sabitine sahip alttaşların fraktal anten tasarımındaki performanslarını sistematik olarak karşılaştırarak, alttaş farkındalıklı anten mühendisliğine katkı sunmakta ve uygulamaya özel anten tasarımı için malzeme seçiminde bir rehber niteliği taşımaktadır.

Anahtar Kelimeler: Fraktal antenler, koch eğrisi, çok bantlı anten, alumina, dielektrik alttaş

ACKNOWLEDGEMENTS

I am deeply grateful to Assistant Professor Gokturk Poyrazoglu for his expert guidance, insightful feedback and continuous support throughout the course of my research. His mentorship played a crucial role in shaping this study.

I would also like to extend my heartfelt thanks to my mother, sister and wife, whose unwavering encouragement, patience and love have been my greatest source of strength. Their support has been instrumental in making this achievement possible.

TABLE OF CONTENTS

LIST OF TABLES

LIST OF FIGURES

LIST OF ACRONYMS AND ABBREVIATIONS

AEU	International Journal of Electronics and Communications
ANSYS	Swanson Analysis Systems
BW	Bandwidth
EU	European Union
e.g	exempli gratia
EPC	Electronic Product Code
FEM	Finite Element Method
FR	Flame Retardant
GRD	Ground Plane Width
HF	High Frequency
HPBW	Half Power Beam Width
HFSS	High Frequency Structure Simulator
IEEE	Institute of Electrical and Electronics Engineer
IFS	Iterated Function Systems
IoT	Internet of Things
ISM	Industrial, Scientific and Medical
Lg	Feedline Width

LTE	Long Term Evolution
PCB	Printed Circuit Board
PNA	Performance Network Analyzer
RF	Radio Frequency
RFID	Radio Frequency Identification
SMA	Subminiature Version A
UHF	Ultra High Frequency
US	United States
USA	United States of America
VSWR	Voltage Standing Wave Ratio
Wi-Fi	Wireless Fidelity
WLAN	Wireless Local Area Networks

1. INTRODUCTION

An antenna is a metallic conductor that is electrically connected to a transmitter or receiver and is responsible for converting electrical signals into electromagnetic waves and vice versa [1]. When current flows through the conductor, alternating magnetic fields are generated, which in turn radiate as electromagnetic waves. Antennas are indispensable components in modern wireless communication systems, including applications such as Radio Frequency Identification and Wireless Local Area Networks (WLAN) [2].

The performance of an antenna is directly related to its geometrical structure, physical dimensions and key parameters such as return loss (S_{11}), gain, bandwidth and input impedance [3]. However, as wireless communication technologies advance, there is a growing demand for compact, efficient and multiband antenna designs. The physical size of an antenna is inherently linked to its operating wavelength, posing a significant design challenge for compact devices [1]. Traditional antenna structures often fail to meet these constraints.

To overcome these limitations, the use of fractal geometries in antenna design has attracted considerable attention in recent years. Fractals are characterized by self similarity and space filling properties, which enable the realization of electrically small antennas capable of multiband operation [4]. Koch curve based fractal antennas, in particular, can increase the effective electrical length of the antenna, allowing reduced physical size while maintaining desirable performance characteristics [5].

One of the most prominent application areas for fractal antennas is RFID systems [6]. These systems are widely employed across sectors such as transportation, logistics, healthcare, banking and access control for the wireless identification of tagged objects. RFID devices are often portable and used in space constrained environments, requiring antennas that are compact, lightweight and efficient across designated frequency bands [7]. Fractal antennas are well suited for such applications due to their low profile design, ease of fabrication, multiband performance and reduced size [4].

In addition to geometry, antenna performance is significantly affected by the properties of the substrate material. The substrate's relative permittivity (ε_r) and loss tangent play a critical role in determining the antenna's resonant frequency, bandwidth, gain and overall radiation efficiency. FR-4 is widely used due to its low cost and ease of availability, although its dielectric performance is limited. On the other hand, Alumina (Al_2O_3), a ceramic based material with a high relative permittivity ($\varepsilon_r \approx 9.8$), low loss tangent and superior thermal and mechanical properties, presents an attractive alternative for high performance antenna applications [8] [9].

In this thesis, a multiband fractal antenna based on the third iteration of the Koch curve is proposed, designed and analyzed. The antenna is developed to operate efficiently at RFID relevant frequencies of approximately 866 MHz, 2.4 GHz and 5.8 GHz. The antenna structures are modeled and optimized using ANSYS HFSS software. A comprehensive parametric analysis is conducted to investigate the influence of key design variables such as ground plane size, feedline width and patch height.

Moreover, the antenna design is implemented on two different substrate materials, FR-4 and Alumina, while maintaining the same geometry, allowing for a direct performance comparison. Simulation results reveal that the Alumina based design enables significant miniaturization and exhibits sharper resonance characteristics, whereas the FR-4 design provides a broader bandwidth but requires a larger physical footprint.

This study contributes to the field of substrate aware antenna engineering by systematically analyzing the impact of substrate materials with different relative permittivity on the performance of fractal antennas. The findings offer valuable insights and practical design guidelines for the development of efficient, compact and multiband antennas tailored for RFID and other modern wireless communication applications.

1.1 Motivation

The rapid advancement of wireless communication technologies has significantly increased the demand for compact, efficient and versatile antenna designs [1]. Devices used in applications such as Internet of Things (IoT), Radio Frequency Identification (RFID) and smart embedded systems are expected to support multiple frequency bands while maintaining a small physical footprint [2] [6]. This requirement poses a major challenge for conventional antenna designs, which often operate in a single frequency band and require considerable space to achieve desirable performance metrics [3].

Fractal antennas have emerged as a promising solution to address this challenge due to their self similar and space filling characteristics [4]. These geometries allow antennas to be miniaturized without compromising their multiband functionality. Koch curve–based antennas, in particular, enable compact designs capable of operating across several frequencies relevant to RFID and wireless communication systems [5] [10].

While geometry plays a critical role in antenna behavior, the effect of substrate material properties such as relative permittivity and loss tangent is equally important [2]. Most existing studies use FR-4 due to its availability and low cost [8]. However, high performance substrates like Alumina (Al_2O_3) offer significantly improved electrical characteristics, potentially allowing for size reduction, enhanced efficiency and better impedance matching [9].

This study is motivated by the need to evaluate and compare the performance of the same fractal antenna structure on two different substrate materials: FR-4 and Alumina. By conducting a detailed simulation based investigation, the study aims to quantify how material properties influence antenna performance in multiband RFID applications. The results will help guide future designers in selecting optimal substrate materials for compact, efficient and cost effective antenna solutions.

1.2 Objective and Scope

The primary objective of this thesis is to design, simulate and evaluate a multiband fractal antenna based on the Koch curve, optimized for RFID and wireless communication applications. A key focus of the study is to investigate the influence of substrate material properties specifically relative permittivity and loss tangent on the performance of the same antenna structure when implemented on two different substrates, FR-4 and Alumina (Al_2O_3).

The scope of the research includes the modeling of the antenna using ANSYS HFSS, conducting parametric analyses on critical geometrical parameters and comparing antenna characteristics such as return loss, bandwidth, gain and radiation patterns. The design is targeted to operate at 866 MHz, 2.4 GHz and 5.8 GHz, which correspond to common RFID and ISM bands [11].

Through a comparative simulation based approach, the study aims to provide insights into how different substrate materials affect antenna miniaturization and performance. The results are intended to serve as a guideline for antenna engineers when selecting substrate materials in compact and multiband wireless systems.

1.3 Literature Review

1.3.1 Fractal Antennas in Modern Wireless Applications

Fractal geometries have emerged as a transformative approach in antenna engineering, particularly where compactness and multiband behavior are required. The concept of fractals structures that exhibit self similarity and possess space filling characteristics was first applied to antenna design by Cohen in the 1990s [12]. These geometries enable antennas to resonate at multiple frequencies while occupying a significantly smaller physical volume than traditional designs [13].

Werner and Mittra conducted a comprehensive study on fractal antenna arrays and explained how iterations of fractal curves like Koch and Sierpinski can increase the effective electrical length of an antenna without increasing its physical size [4]. This makes them especially suitable for compact wireless devices and multiband applications, where antenna footprint is critical.

1.3.2 Koch Curve Geometry and Its Benefits

The Koch curve is one of the simplest and most studied fractal geometries. In each iteration, the number of segments increases, adding complexity and additional current paths, which in turn introduce new resonant frequencies. These characteristics make Koch antennas highly adaptable for multiband communication systems. Several researchers have successfully implemented Koch based antennas in applications ranging from UHF to millimeter wave bands.

For instance, Bahl and Bhartia demonstrated a compact Koch fractal antenna design for passive RFID tags operating in the 860–960 MHz band [14]. Their study highlighted improvements in return loss and impedance matching when compared to traditional monopole and dipole designs.

1.3.3 RFID Antenna Design Requirements

In RFID systems, antennas must be compact, lightweight, low profile and capable of efficient performance at specific frequency bands most commonly 866 MHz (UHF), 2.4 GHz (Wi-Fi/ISM) and 5.8 GHz (industrial applications). Furthermore, RFID tags and readers often operate in embedded, portable or conformal environments, which imposes strict constraints on antenna size and material selection.

Multiband functionality is particularly valuable in RFID, as it allows devices to operate globally (e.g., EU UHF band vs US UHF band) or support multiple protocols. As noted by Brown, achieving multiband behavior with traditional antennas often requires complex switching networks or multiple antennas, increasing cost and size issues that fractal antennas can solve inherently [15].

1.3.4 Substrate Material Effects on Antenna Performance

Beyond geometry, substrate material selection plays a crucial role in antenna design. Parameters such as relative permittivity (ε_r), loss tangent (tanδ) and thickness influence resonant frequency, bandwidth and radiation efficiency. FR-4, while cost effective and widely available, suffers from a high loss tangent and relatively low dielectric stability, making it less suitable for high frequency and precision applications.

Volakis and Sertel discussed how high permittivity materials such as Alumina (Al_2O_3) can enhance antenna performance by reducing size and improving impedance matching and radiation characteristics [16]. Alumina offers superior thermal stability, mechanical rigidity and electrical consistency, making it ideal for high precision, miniaturized antennas in harsh environments.

1.3.5 Literature Gaps and Thesis Contribution

Although extensive research exists on both fractal antennas and substrate material effects, most studies investigate these aspects independently [10] [17]. There is a noticeable lack of systematic comparisons where the same antenna geometry is implemented on different substrates under identical design and simulation conditions [18].

This thesis addresses that gap by designing a Koch curve based multiband fractal antenna and evaluating its performance on both FR-4 and Alumina substrates. By using a controlled simulation environment (ANSYS HFSS) and keeping geometrical parameters constant, the study isolates the impact of substrate materials on antenna performance. The results aim to provide design guidelines and support informed substrate selection for compact RFID antennas in future wireless communication systems.

2. METHODOLOGY AND DESIGN

This chapter presents the methodological and practical foundation of the study, including the antenna design process, employed methods and simulation environment. First, the fundamental performance parameters used to evaluate antenna efficiency are introduced. Then, the structure of the Koch curve based fractal antenna geometry is explained in detail.

The proposed antenna was implemented on two different substrate materials FR-4 and Alumina (Al_2O_3) to analyze and compare their effects on electromagnetic performance. All designs and simulations were carried out using ANSYS HFSS, where parametric analyses were conducted to optimize the key antenna parameters.

This chapter also covers the dielectric properties of the selected substrate materials, the configuration of the simulation environment, boundary conditions, solver settings and mesh generation techniques applied during the HFSS simulations.

2.1 Antenna Performance Parameters

In this section, key antenna performance parameters used for evaluating and optimizing the designed fractal antenna are described. These parameters are critical in determining the efficiency, matching, radiation behavior and suitability of the antenna for specific applications such as RFID and multiband wireless communication systems.

2.1.1 Return Loss (S_{11})

Return loss S_{11} is a fundamental parameter that indicates how much power is reflected back from the antenna input because of impedance mismatch. It is expressed in decibels (dB) and is calculated using the reflection coefficient Γ as:

$$S_{11} = 20 \log_{10} |\Gamma| \tag{2.1}$$

Lower (more negative) values of S_{11} indicate better impedance matching and higher efficiency in power transmission. In most practical antenna designs, a return loss of less than -10 dB is considered acceptable, as it means that more than 90% of the incident power is delivered to the antenna and less than 10% is reflected [19].

Figure 2.1 shows the simulated S_{11} curve for the designed multiband fractal antenna. The antenna demonstrates three distinct resonant frequencies where the return loss dips below the -10 dB threshold. These correspond to the operating frequencies for UHF RFID (around 866 MHz), Wi-Fi/Bluetooth (2.4 GHz) and ISM applications (5.8 GHz). The antenna thus satisfies the multiband operation requirement for typical RFID and wireless communication systems.

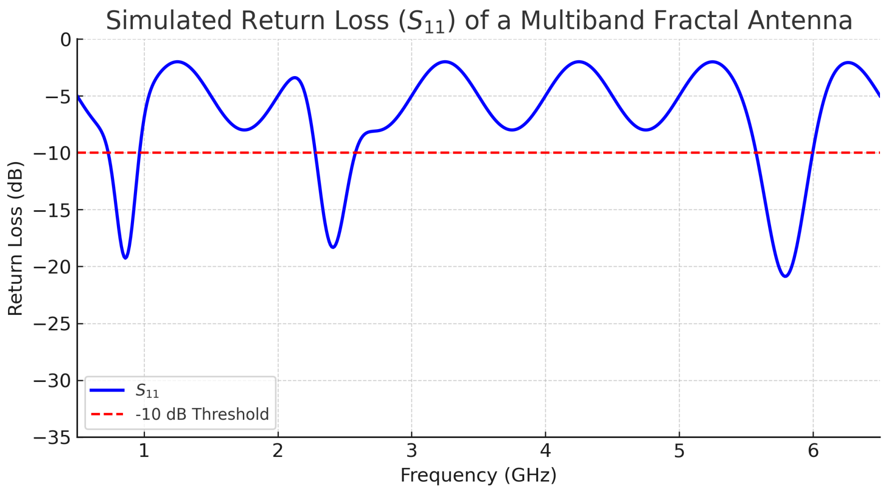

Figure 2.1: *Simulated return loss S_{11} for a multiband fractal antenna. The antenna exhibits resonances at approximately 866 MHz, 2.4 GHz and 5.8 GHz.*

2.1.2 Voltage Standing Wave Ratio (VSWR)

Voltage Standing Wave Ratio (VSWR) is a critical parameter that represents the quality of impedance matching between the antenna and the transmission line. It is derived from the reflection coefficient Γ, which is related to return loss S_{11} and is mathematically expressed as:

$$\mathrm{VSWR} = \frac{1 + |\Gamma|}{1 - |\Gamma|} \tag{2.2}$$

A VSWR of 1.0 indicates perfect matching, where no power is reflected. In practical antenna systems, a VSWR value less than or equal to 2.0 is considered acceptable, which corresponds to return loss values below approximately –9.5 dB [20].

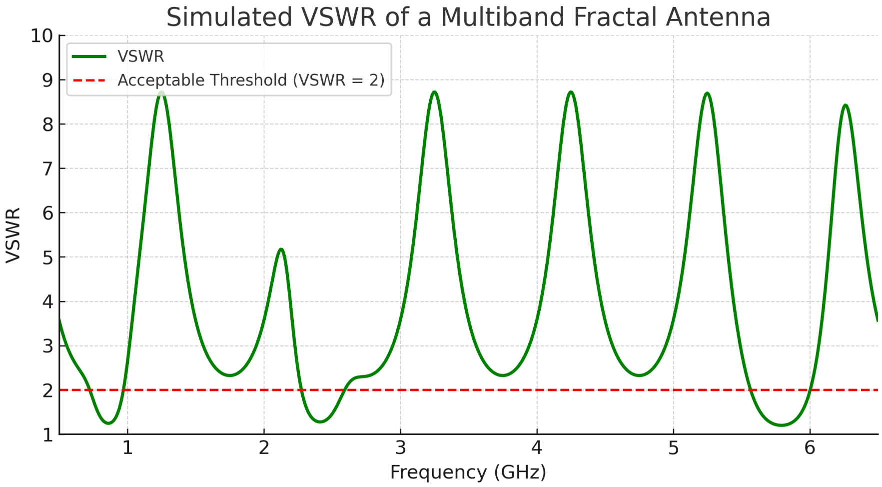

Figure 2.2: *Simulated VSWR response of the multiband fractal antenna. Minimum VSWR values are observed at 866 MHz, 2.4 GHz and 5.8 GHz, indicating good impedance matching.*

Figure 2.2 shows the simulated VSWR curve of the designed multiband fractal antenna. The antenna exhibits low VSWR values, well below 2.0, at the key target frequencies of 866 MHz, 2.4 GHz and 5.8 GHz. This demonstrates efficient power transfer and confirms that the antenna is properly matched to a 50 Ω system at those resonant frequencies.

Maintaining a low VSWR across the desired operating bands is essential for minimizing signal reflections, improving transmission efficiency and ensuring consistent performance in RFID and wireless communication systems.

2.1.3 Bandwidth

Bandwidth is defined as the range of frequencies over which the antenna maintains acceptable performance, typically determined by a specific return loss threshold, commonly $S_{11} < -10$ dB. This indicates that the antenna reflects less than 10% of the incident power and efficiently radiates the remaining energy.

A broader bandwidth allows the antenna to support a wider range of frequencies, which is particularly important in multiband or broadband applications such as RFID, where different regions may operate at slightly different frequency allocations [1].

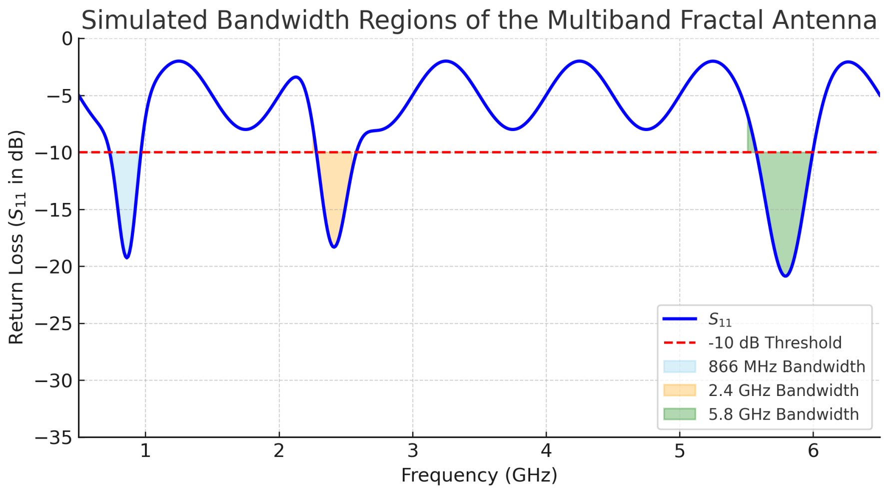

Figure 2.3: *Illustrative representation of bandwidth regions for a multiband antenna where $S_{11} < -10$ dB. Resonances occur around 866 MHz, 2.4 GHz and 5.8 GHz.*

Figure 2.3 demonstrates the frequency intervals where the antenna achieves return loss values below -10 dB. These regions are interpreted as the operational bandwidths for each resonant frequency. In the case of the proposed fractal antenna, the highlighted regions correspond to RFID (866 MHz), Wi-Fi/Bluetooth (2.4 GHz) and ISM applications (5.8 GHz).

Well defined and stable bandwidths are essential for robust communication performance, especially in systems that demand high reliability and consistent link quality across different environments or device configurations.

2.1.4 Radiation Efficiency

Radiation efficiency is a fundamental parameter that quantifies the effectiveness of an antenna in converting input power into radiated electromagnetic energy. It is defined as the ratio of the radiated power (P_{rad}) to the total input power (P_{in}) supplied to the antenna and is mathematically expressed as

$$\eta_{\text{rad}} = \frac{P_{\text{rad}}}{P_{\text{in}}} \tag{2.3}$$

This ratio reflects the portion of input power that is successfully radiated into space, excluding losses due to impedance mismatches, conductor resistance and dielectric heating [21] [22]. Impedance mismatches between the antenna and the transmission line can cause a portion of the power to be reflected back toward the source, thereby reducing efficiency. Additionally, conductor losses occur due to the inherent resistance of metallic components, which dissipate energy in the form of heat. Dielectric losses arise from the lossy nature of the substrate materials used in antenna fabrication.

High efficiency antennas are essential in modern communication systems, particularly in applications such as RFID, IoT and wireless sensor networks, where power consumption must be minimized while maintaining reliable performance. An efficient antenna ensures optimal radiation with minimal internal power dissipation, making it a key design consideration in compact and low power systems [23] [3].

2.1.5 Antenna Efficiency

Antenna efficiency (η_{ant}) represents the overall efficiency of an antenna by considering both the radiation efficiency and the impedance mismatch losses that occur between the antenna and the transmission line [23]. It indicates how effectively the power delivered to the antenna is converted into radiated electromagnetic energy [3].

While radiation efficiency accounts only for conductor and dielectric losses within the antenna structure, antenna efficiency also incorporates the fraction of power that is reflected back due to impedance mismatch [21]. This overall efficiency is expressed mathematically as:

$$\eta_{\text{ant}} = \eta_{\text{rad}} \cdot (1 - |\Gamma|^2) \tag{2.4}$$

where η_{rad} is the radiation efficiency and $|\Gamma|$ is the reflection coefficient at the antenna input. The term $(1 - |\Gamma|^2)$ represents the matching efficiency, which quantifies the proportion of power that is actually accepted by the antenna after reflection losses [22].

In practical antenna systems, both radiation and matching efficiencies significantly affect the total performance. Even if an antenna exhibits high radiation efficiency, a poor impedance match can lead to substantial power being reflected back to the source, thereby lowering the overall antenna efficiency. Conversely, a well matched but lossy antenna will also exhibit reduced efficiency due to internal power dissipation [23].

Achieving high antenna efficiency is essential in modern wireless systems such as RFID, IoT and low power communication networks, where both power conservation and reliable performance are critical [6]. Proper impedance matching and the use of low loss materials are key design strategies to maximize overall antenna efficiency [11].

2.1.6 Gain

Antenna gain describes the ability of the antenna to radiate energy more effectively in a particular direction compared to an isotropic source. It is typically expressed in decibel isotropic (dBi). Higher gain values indicate a more focused beam, which is particularly desirable in RFID readers, directional communication systems or point to point wireless links [2].

Mathematically, gain is defined as Equation 2.5, where η represents the radiation efficiency and $D(\theta, \phi)$ is the directivity of the antenna [2]:

$$G(\theta, \phi) = \eta \cdot D(\theta, \phi) \tag{2.5}$$

Radiation efficiency represents the fraction of the input power that is converted into radiated energy, accounting for conductor and dielectric losses [23]. It does not include mismatch losses. Antenna efficiency, on the other hand, considers both radiation efficiency and matching efficiency, providing a more realistic measure of the antenna's overall performance [3]. Even if an antenna has high directivity, poor radiation or matching efficiency can reduce its overall gain [21].

As shown in Figure 2.4, the 3D radiation pattern illustrates the main lobe of the fractal antenna pointing along the z axis. The main lobe indicates the direction of maximum radiation. This directional behavior implies that the antenna is optimized to radiate more energy in one direction, which is beneficial for increasing range and improving link reliability in focused applications [24].

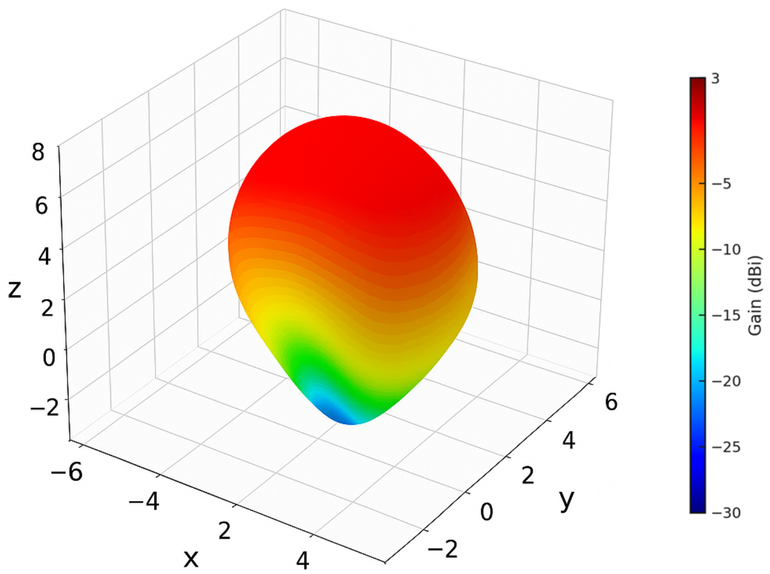

Figure 2.4: *Illustrative 3D radiation pattern showing the directional gain of the fractal antenna*

The shape and direction of the gain pattern are directly influenced by the antenna geometry, substrate material and operating frequency [25]. These characteristics will be further examined in the simulation results section to evaluate how the fractal geometry and substrate selection affect antenna gain at each resonant frequency.

2.1.7 Radiation Pattern

The radiation pattern of an antenna represents the variation of radiated power as a function of direction in space. It is commonly visualized in 2D or 3D plots, using spherical coordinates where the angular variation in the E-plane and H-plane is displayed. These patterns are critical for understanding how the antenna focuses or distributes energy in specific directions [23].

For planar antennas, 2D polar plots are typically used to illustrate the E-plane (electric field plane) and H-plane (magnetic field plane) responses. Omnidirectional antennas exhibit circular patterns in one plane, whereas directional antennas produce lobed shapes as in Figure 2.5, concentrating radiation in particular angles. This shape is an illustrative E-plane radiation pattern of a directional antenna, while nulls (minimal radiation) occur perpendicular to that axis [2].

Understanding the radiation pattern is essential for antenna placement, orientation and application targeting [6]. It ensures that energy is radiated efficiently toward intended directions, which is important for systems such as RFID readers, point to point wireless links or sensor arrays.

2.1.8 Input Impedance

Input impedance is a key parameter that defines how much opposition an antenna presents to the input signal at its feed point. It is a complex quantity, typically expressed as Equation 2.6, where R is the resistive (real) part and X is the reactive (imaginary) part of the impedance [3]:

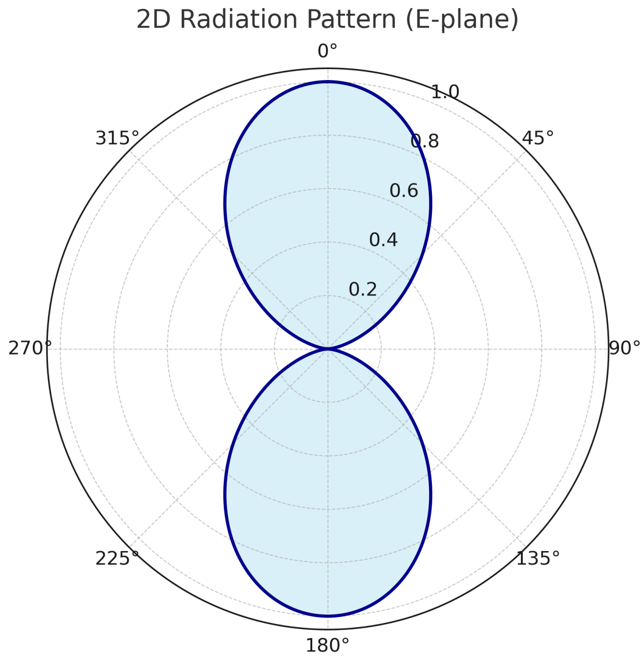

Figure 2.5: *Illustrative 2D radiation pattern in the E-plane. Figure indicates directional radiation with nulls at 90° and 270°.*

$$Z_{\text{in}} = R + jX \tag{2.6}$$

Ideally, for efficient power transfer in most RF and microwave systems, the antenna should match the characteristic impedance of the transmission line, usually 50 Ω [23]. If $Z_{\text{in}} = 50 + j0\ \Omega$, the antenna is perfectly matched. A mismatch causes power to reflect back to the source and reduces system efficiency [19].

Impedance mismatch can be quantified using return loss or VSWR and is often visualized using a Smith Chart or plotted as real and imaginary components over frequency. Proper input impedance ensures minimal signal reflection and maximum radiation efficiency. During antenna design, impedance matching is typically achieved by adjusting antenna geometry or using matching networks [22]. In this study, the designed fractal antenna was optimized to achieve input impedance values close to 50 Ω at the target resonant frequencies of 866 MHz, 2.4 GHz and 5.8 GHz.

2.1.9 Half Power Beam Width (HPBW)

Half Power Beam Width (HPBW) is a measure of the angular spread of the main lobe of an antenna's radiation pattern. It is defined as the angular range between the points where the radiated power drops to half of its maximum value, corresponding to a –3 dB drop in gain [3].

HPBW is typically measured in either the E-plane or H-plane and is used to quantify the directivity and focus of the antenna [24]. A narrow HPBW indicates a highly directional antenna with concentrated energy in a limited angular region, whereas a wide HPBW implies broader coverage [25].

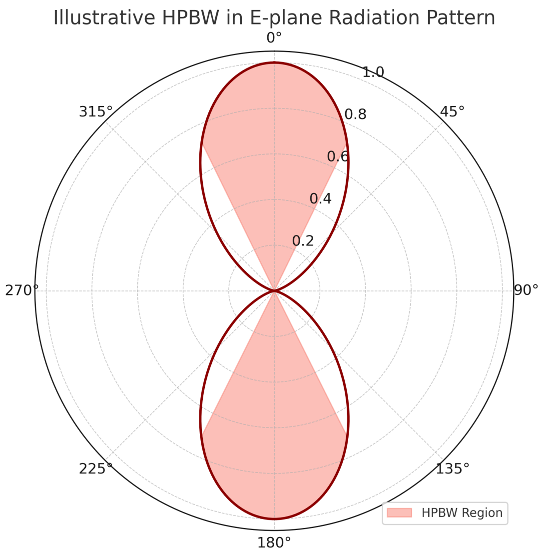

Figure 2.6: *Illustrative E-plane radiation pattern showing Half Power Beam Width (HPBW) region shaded between –3 dB points.*

As illustrated in Figure 2.6, the HPBW is represented by the angular span of the main lobe between the two –3 dB points relative to the peak gain. This parameter helps determine how narrowly or broadly the antenna directs its energy [3].

In practical applications such as RFID readers or directional wireless links, a smaller HPBW is beneficial for targeting specific areas or minimizing interference, while wider HPBW is preferred for omnidirectional coverage [6].

2.2 Antenna Polarization

Antenna polarization refers to the orientation and trajectory of the electric field vector of the electromagnetic wave radiated by an antenna. In a specific direction, the polarization of an antenna is defined as the polarization of the wave it radiates in that direction. Since electromagnetic waves consist of both electric and magnetic fields, polarization is concerned primarily with the time varying direction of the electric field vector, as it is more easily influenced by the design and orientation of the antenna [23].

Polarization can be classified into three main types: linear, circular and elliptical. In linear polarization, the electric field vector maintains a constant direction, either horizontal or vertical, over time. Circular polarization occurs when the electric field rotates in a circular motion, forming a helical trajectory; it is considered right hand or left hand depending on the rotation direction [2]. Elliptical polarization is the most general case, where the tip of the electric field vector describes an ellipse over time. Both circular and linear polarizations are special cases of elliptical polarization [15].

Polarization matching between the transmitting and receiving antennas is crucial for efficient power transfer. Mismatched polarization can lead to polarization losses, significantly reducing the received signal strength [6]. Therefore, polarization plays a critical role in the design and placement of antennas in systems such as satellite communication, RFID and mobile networks [11].

3. FRACTAL GEOMETRY

3.1 Introduction to Fractal Geometry in Nature

Fractal geometry is a modern mathematical framework that extends beyond classical Euclidean geometry and is used to describe complex, irregular and self similar structures frequently found in nature. The concept was first introduced by Benoît B. Mandelbrot in 1975 and popularized through his seminal work *The Fractal Geometry of Nature*. The term ”fractal” is derived from the Latin word *fractus*, meaning broken or fragmented [26].

Fractals are characterized by structures that repeat themselves at multiple scales and exhibit unique mathematical and geometrical properties, such as self similarity, fractional dimension and infinite complexity. These features make them highly suitable for various scientific and engineering applications, including image compression, modeling natural phenomena and antenna design [27].

One of the most fascinating aspects of fractal geometry is its presence in numerous natural structures [28]. From biological formations to geological features, nature provides an abundance of recursive and self similar patterns that illustrate the principles of fractal mathematics [29] [30]. Below are several real world examples of naturally occurring fractals, displayed in Figure 3.1.

***(a)** Romanesco Broccoli [28]* ***(b)** Lightning [29]* ***(c)** Leaf [30]*

Figure 3.1: *Examples of fractal patterns in nature*

These natural examples demonstrate that fractals are not merely abstract mathematical concepts but practical tools for interpreting the complexity of the physical world. Their underlying principles inspire the development of artificial fractal structures, including antennas, which benefit from their compact size and multiband behavior.

3.1.1 Key Properties of Fractal Structures

Fractal structures exhibit several fundamental properties that distinguish them from classical shapes:

- Self Similarity: A fractal object resembles itself at different scales [27]. This similarity may be exact (as in the Sierpinski triangle) or statistical (as in natural coastlines).
- Scale Invariance: The structure looks similar regardless of the magnification level [26], which allows fractal based antennas to operate efficiently over multiple frequencies.
- Infinite Complexity: Fractals can be generated through an infinite number of iterations, increasing geometrical detail at each step [27].
- Fractional Dimension: Fractals have noninteger dimensions, which quantify their spatial complexity. For instance, the Koch curve has a fractal dimension of approximately 1.26 [31].

3.1.2 Relevance of Fractals in Electromagnetic Applications

Fractal geometries are particularly valuable in electromagnetic engineering due to their ability to create compact, multiband and wideband antenna structures. The self similarity and space filling nature of fractals allow designers to increase electrical length without increasing physical size. They also allow introduction of multiple resonant paths through iterative geometry [24]. Fractals support multiband or broadband operation with a single element. Furthermore, they achieve compact form factors suitable for embedded systems [25].

These characteristics make fractal antennas especially useful in applications where size, weight and multiband performance are critical [14]. They are particularly suitable for RFID tags [6]. They are used in Wi-Fi modules [25]. Fractal antennas are beneficial for satellite communication systems [4]. They are also employed in implantable medical devices [10].

3.2 Fractal Antennas

In modern communication systems, antenna design is increasingly challenged by the demands for compactness, multi frequency operation and high efficiency. In conventional antenna structures, the physical dimensions are tightly coupled to the wavelength corresponding to the desired operating frequency, typically on the order of $\lambda/2$ or $\lambda/4$. This physical constraint limits the integration of antennas into portable and embedded systems [20]. Fractal geometry, with its inherent properties of self similarity, scale invariance and space filling behavior, offers a promising alternative to address these limitations. Fractal antennas, designed based on such geometries, present a novel solution by enabling multiband, wideband and miniaturized antenna designs.

A fractal antenna is constructed by applying a recursive geometrical transformation to a basic shape, called the initiator, using a generator that introduces a repetitive structure at every iteration. Each successive iteration increases the electrical length of the antenna without proportionally increasing its physical size. As a result, the antenna can resonate at multiple frequencies, each iteration contributing new current paths that generate distinct resonances [5]. The increased geometrical complexity also enhances other electromagnetic characteristics such as impedance matching, gain and radiation efficiency [24].

Several types of fractal geometries have been widely studied and applied in antenna engineering [10]. Among these, the Koch curve is one of the most commonly used due to its simplicity and excellent multiband behavior. It is generated by successively modifying a straight line segment by inserting equilateral triangle protrusions at each iteration step, thereby increasing the effective path length. Other notable geometries include the Sierpinski triangle, which is suited for log periodic and frequency scaled structures [5]. The Hilbert and Peano curves are space filling and enable compact designs [4]. The Minkowski island is often employed to improve bandwidth in microstrip antennas [32].

The advantages offered by fractal antennas go beyond geometry. They also exhibit distinct electromagnetic benefits. A well designed fractal antenna can display multiple deep nulls in the return loss S_{11} plot, indicating strong impedance matching at multiple frequency bands. The radiation pattern and directional characteristics can also be influenced by the fractal's symmetry and iteration level. Depending on the specific geometry, fractal antennas can exhibit either omnidirectional or directional radiation patterns, making them adaptable to various application scenarios [2]. Figure 3.2 shows examples of fractals created by using mathematical expressions.

Fractal antennas have found applications across a broad range of domains [4]. In RFID systems, their compact size and multiband behavior make them suitable for tag antennas operating at UHF and HF bands [14]. In mobile devices, a single fractal antenna can support multiple standards such as Wi-Fi, LTE and Bluetooth [25]. In satellite communication, the ability to maintain high gain in a compact form factor is a significant advantage [4]. Furthermore, in biomedical applications, fractal antennas are employed in implantable or wearable systems due to their small size and efficient operation in low

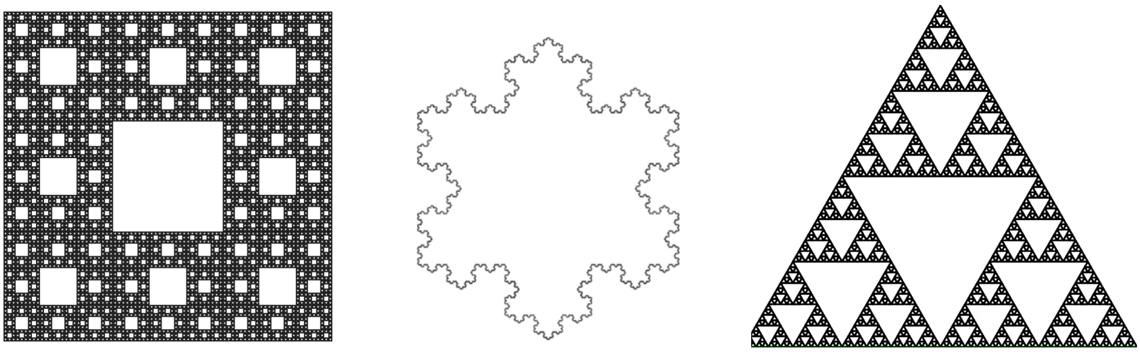

***(a)** Sierpinski Carpet [5]* ***(b)** Koch Snowflake [31]* ***(c)** Sierpinski Triangle [5]*

Figure 3.2: *Some fractal examples, from left to right: Sierpinski Carpet, Koch Snowflake, Sierpinski Triangle*

power environments [10]. These diverse applications demonstrate that fractal antennas offer scalable, flexible and high performance solutions for the next generation of wireless systems [24].

3.3 Generation of Fractals Using Iterated Function Systems (IFS)

Fractals can be generated through an iterative mathematical approach known as the *Iterated Function System (IFS)* [26]. This method involves repeatedly applying affine transformations to a basic geometric shape (the initiator) to generate a self similar structure with increasing complexity. Affine transformations combine scaling, rotation, reflection and translation in a two dimensional plane and are fundamental to constructing many classical fractals [31].

An affine transformation w can be expressed in matrix form as follows:

$$w\begin{pmatrix} x \\ y \end{pmatrix} = \begin{pmatrix} a & b \\ c & d \end{pmatrix}\begin{pmatrix} x \\ y \end{pmatrix} + \begin{pmatrix} e \\ f \end{pmatrix} \tag{3.1}$$

Here, the coefficients a and d represent scaling, b and c correspond to rotation and shear, e and f define translation along the x and y axes, respectively.

The process of generating a fractal shape involves applying a finite set of affine transformations $\{w_1, w_2, \ldots, w_n\}$ to the initial geometry A_0, resulting in successive sets:

$$A_1 = W(A_0) \tag{3.2}$$

$$A_2 = W(A_1) \tag{3.3}$$

$$\vdots \tag{3.4}$$

$$A_{k+1} = W(A_k) \tag{3.5}$$

where W is the union of all individual transformations:

$$W(A) = \bigcup_{i=1}^{n} w_i(A) \tag{3.6}$$

As $k \to \infty$, this iterative process converges to a fixed structure A:

$$\lim_{k\to\infty} A_k = A, \quad \text{where } W(A) = A \tag{3.7}$$

This process forms the mathematical foundation of many well known fractals, including the Koch curve. For the Koch curve, the initial line segment is transformed by four affine functions, each of which creates one of the four parts of the characteristic snowflake motif. The procedure is then repeated recursively on each resulting segment [31].

An example of a Koch curve construction using four affine transformations is illustrated in Figure 3.3, where each transformation alters the geometry according to specific scale, rotation and translation parameters. After the first iteration (A_1), the same set of transformations is applied to all resulting segments to obtain the second iteration (A_2) and so forth.

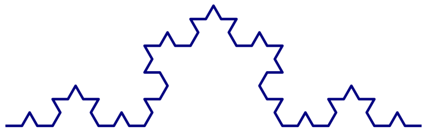

Figure 3.3: *Third iterations of the Koch fractal curve using IFS.*

3.4 Koch Fractal Generation using Affine Transformations

The Koch curve is a well known example of a self similar fractal constructed using Iterated Function Systems (IFS) [31]. This method involves repeatedly applying affine transformations to a line segment in order to generate increasingly complex and space filling structures [33] [34]. An affine transformation combines scaling, rotation and translation in a two dimensional space and can be represented as in Equation 2.1 [31].

To generate the Koch curve, four specific affine transformations $\{w_1, w_2, w_3, w_4\}$ are applied to the initial segment A_0 [34]. These transformations define how each segment is scaled, rotated and translated to create the next iteration A_1:

$$w_1(x, y) = \begin{pmatrix} \frac{1}{3} & 0 \\ 0 & \frac{1}{3} \end{pmatrix} \begin{pmatrix} x \\ y \end{pmatrix} + \begin{pmatrix} 0 \\ 0 \end{pmatrix} \tag{3.8}$$

$$w_2(x, y) = \begin{pmatrix} \frac{1}{6} & -\frac{\sqrt{3}}{6} \\ \frac{\sqrt{3}}{6} & \frac{1}{6} \end{pmatrix} \begin{pmatrix} x \\ y \end{pmatrix} + \begin{pmatrix} \frac{1}{3} \\ 0 \end{pmatrix} \tag{3.9}$$

$$w_3(x, y) = \begin{pmatrix} \frac{1}{6} & \frac{\sqrt{3}}{6} \\ -\frac{\sqrt{3}}{6} & \frac{1}{6} \end{pmatrix} \begin{pmatrix} x \\ y \end{pmatrix} + \begin{pmatrix} \frac{1}{2} \\ \frac{\sqrt{3}}{6} \end{pmatrix} \tag{3.10}$$

$$w_4(x, y) = \begin{pmatrix} \frac{1}{3} & 0 \\ 0 & \frac{1}{3} \end{pmatrix} \begin{pmatrix} x \\ y \end{pmatrix} + \begin{pmatrix} \frac{2}{3} \\ 0 \end{pmatrix} \tag{3.11}$$

Each transformation w_i maps the unit segment to a part of the Koch curve [33]. The union of these mappings constructs the new set of segments:

$$W(A) = \bigcup_{i=1}^{4} w_i(A) \tag{3.12}$$

Through recursive application of W on the initial geometry A_0, the Koch fractal curve is formed [34]:

$$W(A) = \left(\begin{array}{cccc|cc} \frac{1}{3} & 0 & 0 & \frac{1}{3} & 0 & 0 \\ \frac{1}{6} & -\frac{\sqrt{3}}{6} & \frac{\sqrt{3}}{6} & \frac{1}{6} & \frac{1}{3} & 0 \\ \frac{1}{6} & \frac{\sqrt{3}}{6} & -\frac{\sqrt{3}}{6} & \frac{1}{6} & \frac{1}{2} & 0 \\ \frac{1}{3} & 0 & 0 & \frac{1}{3} & \frac{2}{3} & 0 \end{array}\right) \tag{3.13}$$

Figure 3.4 illustrates the evolution of the Koch curve from the initial segment to the third iteration. Each stage demonstrates how affine transformations introduce additional geometric detail, leading to the self similar and complex structure characteristic of fractals [31].

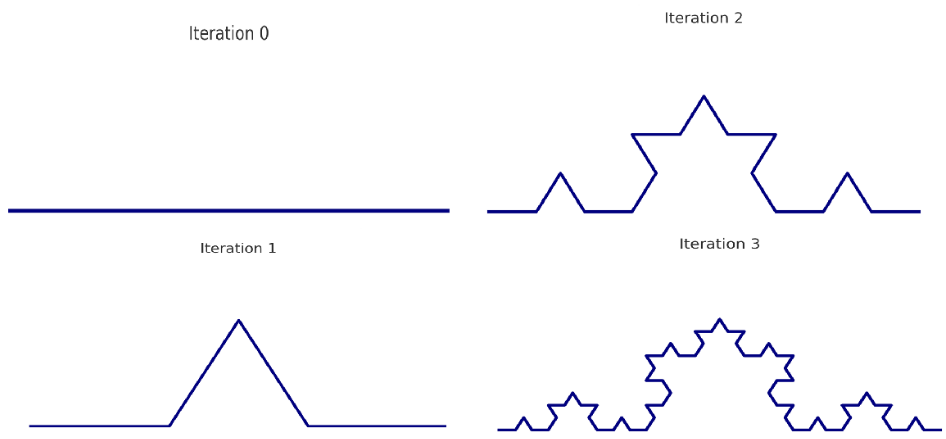

Figure 3.4: *Construction of the Koch curve from iteration 0 (a straight line) to iteration 3 using IFS based affine transformations.*

The matrix representation given in Equation (3.13) compactly expresses the four affine transformations that define the first iteration of the Koch fractal curve. Each row in the matrix corresponds to one affine transformation function w_i and each function is composed of a linear transformation matrix and a translation vector. Specifically, the first two columns of each row represent the first row of the linear part A_i, the next two columns represent the second row of A_i and the final two columns correspond to the translation vector $\mathbf{t}_i = (e_i, f_i)$. This compact matrix notation enables the entire set of transformations to be visualized in a single structure. The affine transformations include combinations of scaling, rotation and translation, applied to the initial line segment to generate the first level geometry. As the process is recursively repeated, each segment is further subdivided and transformed according to the same set of functions, producing an increasingly detailed and self similar geometry that converges to the Koch curve in the limit. This approach demonstrates the power and elegance of Iterated Function Systems (IFS) in fractal generation and is particularly effective for modeling fractal based antenna structures.

4. FRACTAL ANTENNA DESIGN AND SIMULATION RESULTS

This chapter provides a comprehensive overview of the design methodology used for developing and analyzing the proposed fractal antenna. The process begins with the selection of an appropriate fractal geometry. Specifically, the Koch snowflake, which is known for its self similar structure and space filling properties, making it suitable for compact and multiband antenna applications. Following the geometric design, the antenna is modeled and simulated using ANSYS HFSS, a 3D full wave electromagnetic solver based on the Finite Element Method (FEM). The simulation environment enables precise analysis of return loss, radiation characteristics and gain at different frequency bands. Additionally, the impact of using different dielectric substrates, namely FR-4 and Alumina, is investigated to evaluate how material properties influence the antenna's electromagnetic performance. Through parametric simulation, the antenna is fine tuned to operate effectively within RFID and ISM frequency bands. Each phase of the design and simulation process is discussed in detail in the subsequent sections.

4.1 Design Overview

The Koch fractal geometry is selected for this design due to its inherent self similarity and space filling characteristics, which enable the creation of compact structures with extended electrical length. Each iteration of the Koch curve introduces additional segments and sharp corners, effectively increasing the current path within a fixed physical area. This behavior allows the antenna to support multiple resonant frequencies without significantly increasing its size, making it well suited for applications that require multiband performance in limited space. Additionally, the simplicity of the Koch construction facilitates easy implementation in simulation tools and practical fabrication using standard PCB manufacturing techniques. These properties make the Koch fractal an attractive candidate for modern wireless communication systems where compactness, bandwidth and frequency agility are key design objectives.

4.2 Design of Compact Multiband Fractal Monopole Antenna with FR-4 Substrate

The proposed compact multiband monopole antenna, based on the third iteration of Koch fractal geometry, has been simulated using ANSYS HFSS. The simulations were carried out using an FR-4 substrate with a thickness of 1.6 mm and a relative permittivity of $\varepsilon_r = 4.4$. The performance was evaluated through return loss S_{11}, radiation characteristics and parametric studies to optimize key design parameters.

Figure 4.1 illustrates the physical layout of the proposed antenna. The design employs the third iteration of the Koch curve as the radiating element, enabling extended electrical length within a compact footprint. The feedline is a microstrip line optimized for 50 Ohm matching and the ground plane is partially reduced to enhance radiation performance. The overall geometry supports multiband operation by incorporating multiple resonant paths through fractal segmentation. The radiating patch incorporates fractal edges, the ground plane and feedline are tuned to optimize impedance matching and gain.

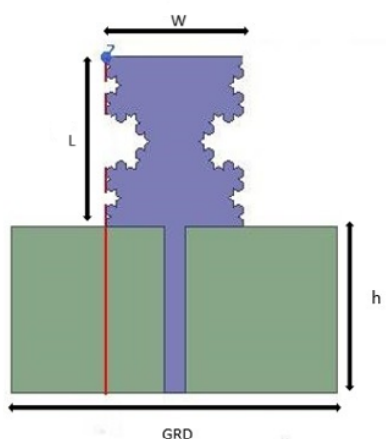

Figure 4.1: *Geometry of the proposed third iteration Koch fractal monopole antenna*

To determine the effect of fractal iteration, antennas based on the first, second and third iterations of the Koch curve were modeled. As depicted in Figure 4.2, the third iteration significantly enhances the multiband behavior of the antenna. Unlike the lower iterations, it introduces additional resonant frequencies and wider impedance bandwidths, thereby making it more suitable for RFID and ISM band applications. This justifies the selection of the third iteration as the basis for the final antenna design.

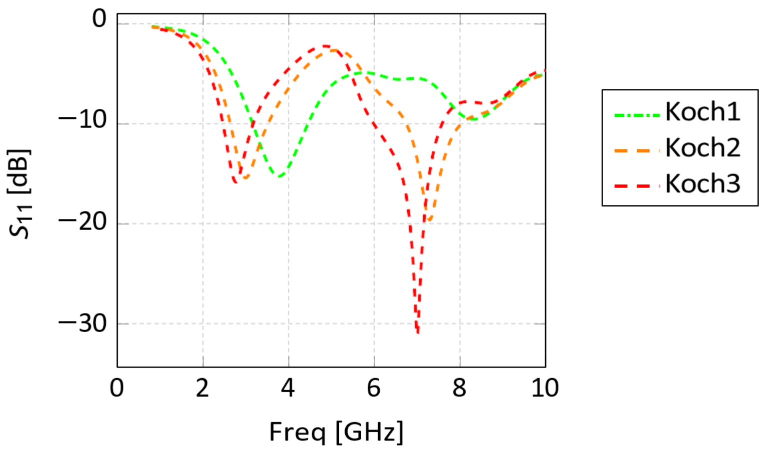

Figure 4.2: *Simulated S_{11} comparison for Koch fractal antennas with first, second and third iteration geometries.*

After selecting the optimal fractal structure, several parametric studies were performed to assess the influence of physical dimensions on antenna behavior. In particular, the effects of ground plane width (GRD), feedline width (Lg) and feedline height (h) were examined.

As shown in Figure 4.3, changing the width of the ground plane from 25 mm to 55 mm has a noticeable effect on the upper frequency bands, while the lower band around 2.4 GHz remains relatively stable. A narrower ground plane introduces stronger coupling and enables more efficient excitation of higher order modes, enhancing the upper band return loss. However, excessively reducing the ground can compromise radiation efficiency.

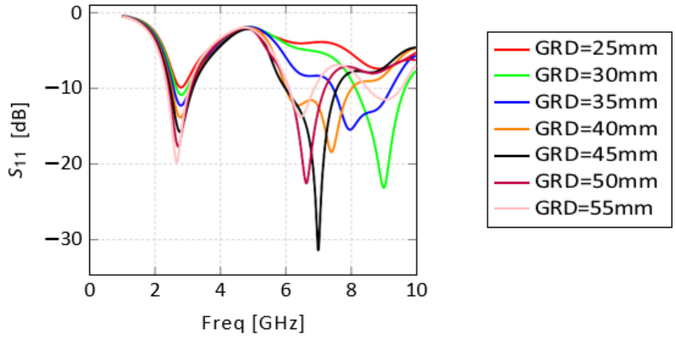

Figure 4.3: *S_{11} results for different ground plane widths. Improved matching is observed around 5.8 GHz as the GRD is optimized.*

Similarly, the feedline width (Lg) has been swept from 2 mm to 6 mm. According to the results in Figure 4.4, increasing Lg reduces the input impedance, leading to downward frequency shifts and reduction in bandwidth. A width of 4 mm was determined to offer the best compromise between impedance matching and manufacturability.

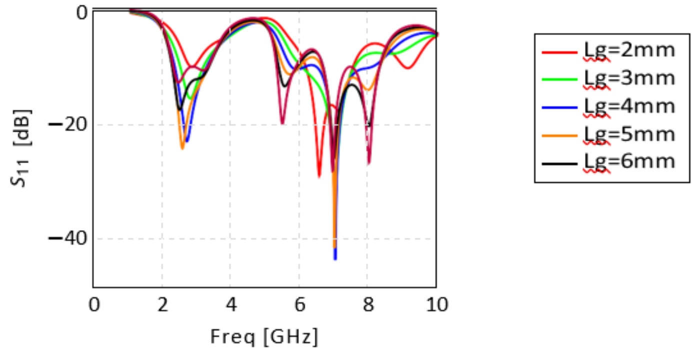

Figure 4.4: *S_{11} performance for different feedline widths. Wider lines reduce impedance, shifting resonant frequencies.*

In Figure 4.5, feedline height (h) is varied. It is found that increasing h lowers the resonant frequencies due to increased electrical length. However, very tall structures can degrade pattern stability, which is critical for portable and wearable applications. Therefore, a height of 20 mm was chosen based on the tradeoff between resonance control and mechanical practicality.

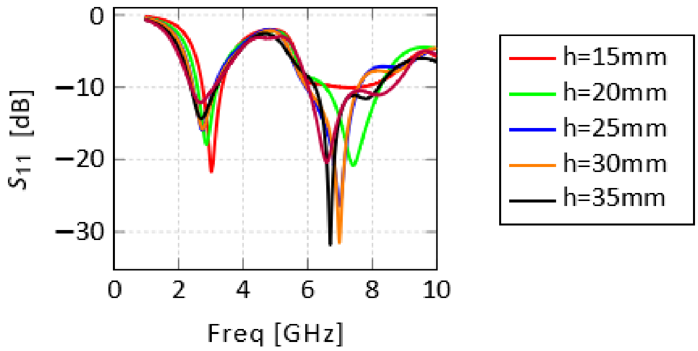

Figure 4.5: *Variation of S_{11} response with feedline height (h). Height directly affects resonance positions.*

The final optimized antenna design exhibits excellent impedance matching at both 2.4 GHz and 5.8 GHz, with return loss values below –10 dB. This confirms that the antenna efficiently radiates and receives at those frequencies, which are widely used in IoT and Wi-Fi systems.

Table 4.1: *Proposed antenna dimensions*

Parameter	Optimized Size (mm)
L	21.00
W	18.93
GRD	45.00
h	20.00
Lg	3

The parameters L (length of radiator), W (width of radiator), GRD (ground plane width) and h (height of feedline) were optimized through iterative HFSS simulations to achieve better impedance matching and multiband performance.

The final S_{11} graph of the fractal antenna created with the determined parameters is shared in the Figure 4.6.

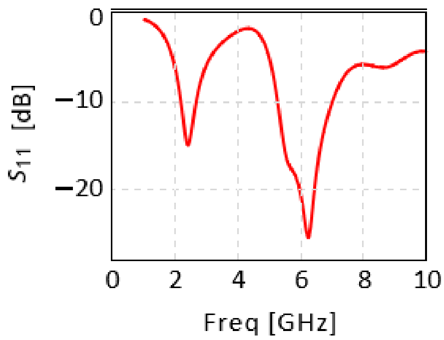

Figure 4.6: *The S_{11} responses of the third iteration Koch fractal monopole antenna*

In terms of radiation performance, the 2D polar plots shown in Figures 4.7 and 4.8 illustrate the E-plane and H-plane patterns at 2.4 GHz and 5.8 GHz, respectively. At 2.4 GHz, the pattern is more omnidirectional, which is ideal for general wireless coverage, while at 5.8 GHz the pattern becomes slightly more directive, indicating improved gain and front to back ratio.

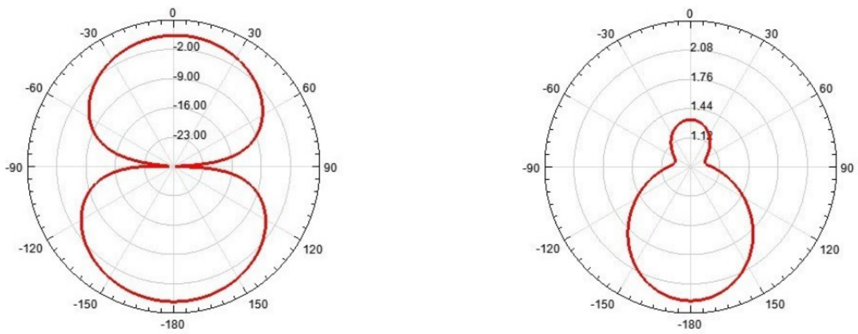

Figure 4.7: *2D radiation patterns at 2.4 GHz. Left: E-plane, Right: H-plane.*

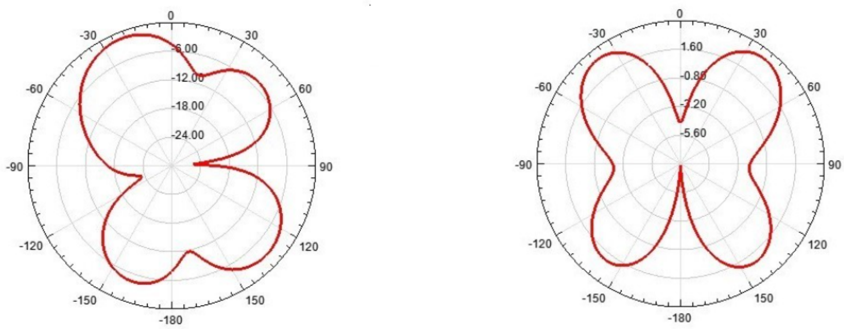

Figure 4.8: *2D radiation patterns at 5.8 GHz. Left: E-plane, Right: H-plane.*

The far field 3D radiation patterns, presented in Figure 4.9, further validate the multiband behavior and directional nature at higher frequencies. The gain at 2.4 GHz was measured to be 2.3 dBi and at 5.8 GHz to be 3.3 dBi, which are satisfactory for compact antenna designs with fractal geometries.

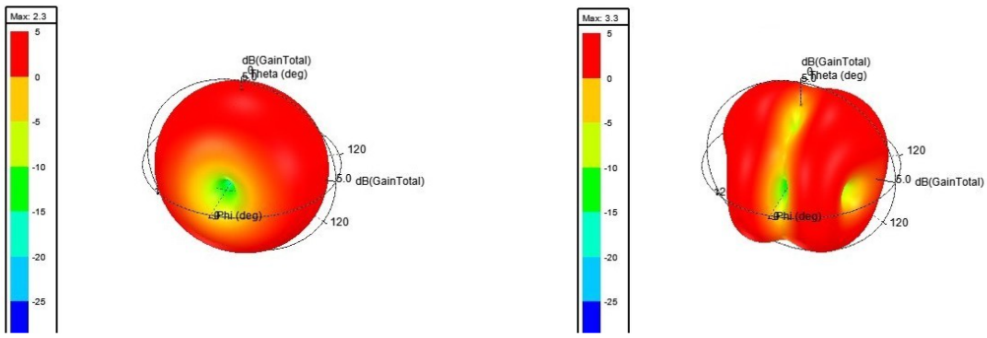

Figure 4.9: *3D radiation patterns of the proposed antenna at 2.4 GHz (left) and 5.8 GHz (right).*

Finally, Table 4.2 summarizes a performance comparison of the proposed antenna with several recently published multiband antennas. As evident, the proposed design achieves competitive bandwidth and gain values while significantly reducing the overall antenna size.

Table 4.2: *Comparison with the recently published literature*

Reference	Size (mm^3)	Resonant Freq. (GHz)	Bandwidth (%)	Gain (dBi)
Ref [25]	30×24.4×1.6	3.1 / 5.52 / 7.31 / 9.72	3.5 / 5.01 / 13.2 / 5.77	1.35 / 1.0 / 1.07 / 1.75
Ref [24]	40×40×1.6	1.5 / 3.5 / 5.4	1.9 / 14 / 5	–4.5 / 3.75 / 5.3
Ref [35]	18.8×20×0.76	2.4 / 5.2	1.6 / 23	–1.7 / 2.4
Ref [36]	40.7×33.4×1.6	2.4 / 5.8	54.52 / 11.80	1.9–2.8 / 5.20–5.65
Proposed	45×41×1.6	2.4 / 5.8	20.8 / 31.8	2.3 / 3.3

4.2.1 Measured Results

Calibration is an essential step in RF measurements to ensure the accuracy and reliability of the results. Before measuring antenna performance, calibration is performed to eliminate systematic errors introduced by the measurement system, including cable losses, connector mismatches and phase distortions. By moving the reference plane to input of antenna, calibration allows for precise characterization of parameters such as return loss and VSWR. Without proper calibration, the measurement data would include unwanted effects from the test setup itself, leading to inaccurate conclusions about the device under test. Therefore, calibration is critical, especially in high frequency applications such as antenna design and evaluation [37].

To experimentally validate the simulation results, the proposed Koch fractal antenna was fabricated on a FR-4 substrate using standard PCB manufacturing techniques. A Sub Miniature version A (SMA) connector with 50 Ohm characteristic impedance was mounted onto antenna structure to perform RF measurements. Measurements were carried out using a Keysight PNA-X Vector Network Analyzer (Model N5242B) after calibration using the Keysight N4691B electronic calibration module, as shown in Figure 4.10. The frequency sweep was configured from 10 MHz to 10 GHz with a power level of –5 dBm and 451 sweep points. In Figure 4.11, the fabricated antenna can also be seen while the measurement is being taken.

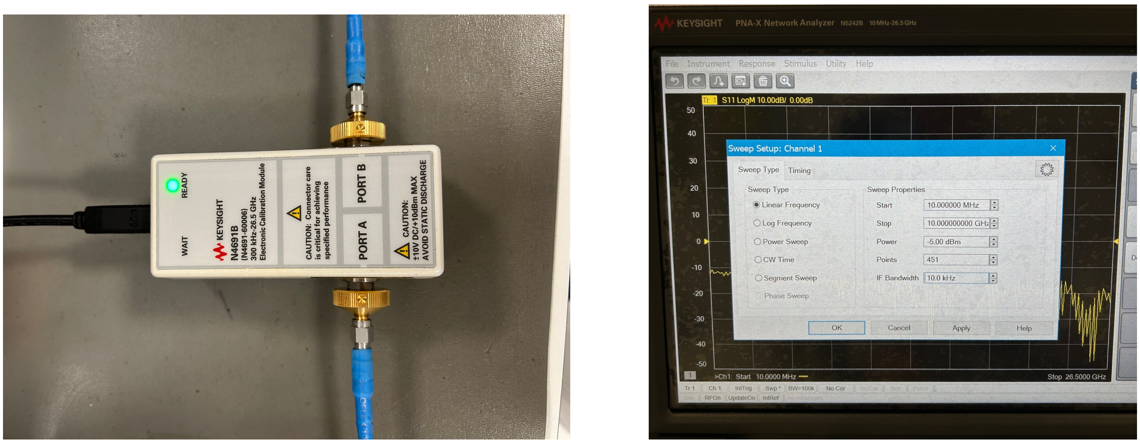

Figure 4.10: *Electronic calibration setup and Sweep configuration screen of the Keysight PNA-X Vector Network Analyzer*

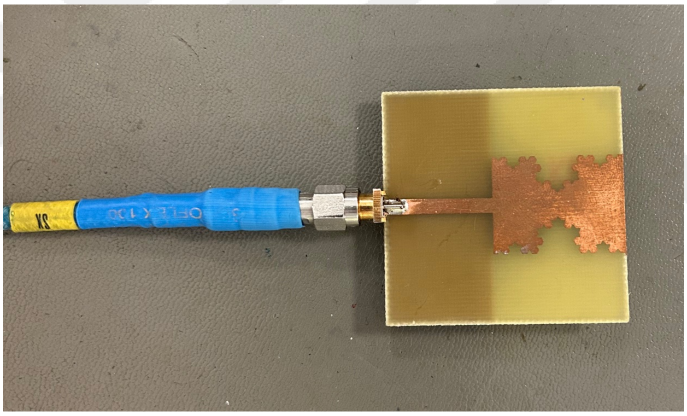

Figure 4.11: *Photograph of the fabricated Koch fractal antenna*

The measured return loss S_{11} of the fabricated antenna is shown in Figure 4.12. These results show strong agreement with the simulation results presented earlier. In particular, the presence of a deep resonance near 6 GHz in both measured and simulated S_{11} curves confirms the effectiveness of the third iteration Koch fractal geometry in enabling multiband operation. The minor shifts in frequency and depth are attributed to manufacturing tolerances and slight variations in material properties. Nevertheless, the antenna demonstrates reliable multiband performance with return loss values below –10 dB at all target frequencies. The S_{11} results obtained from the network analyzer are summarized in Table 4.3, indicating frequencies 2.4 GHz, 5.8 GHz and the deep point of the graph.

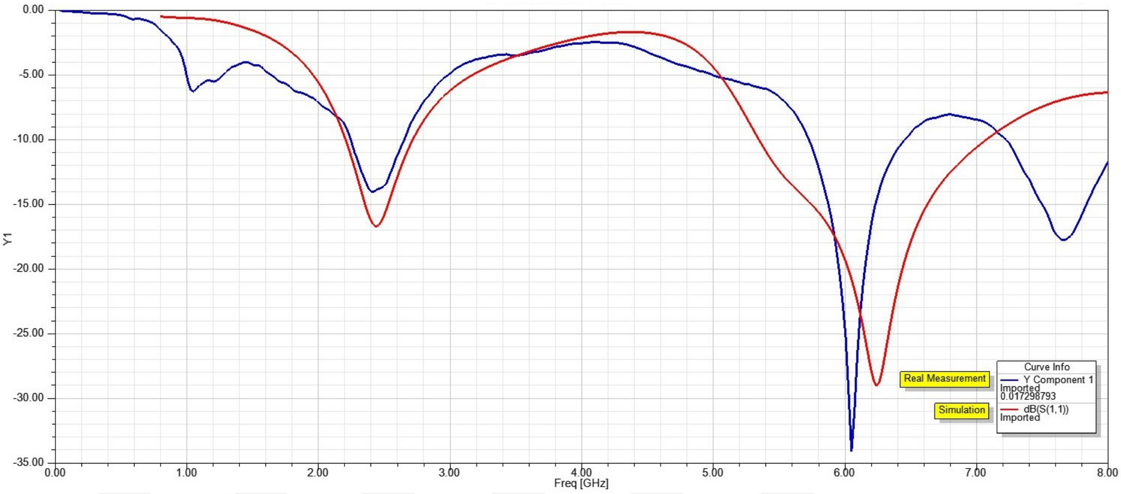

Figure 4.12: *The S_{11} responses of the fabricated and simulated antennas*

Table 4.3: *Measured S_{11} values*

Frequency (GHz)	Return Loss (dB)
2.40	–13.98
5.80	–12.20
6.05	–33.83

4.2.2 Comparison Between Simulated and Measured Results

A comparison between the simulated and measured S_{11} responses of the Koch fractal antenna is presented in Table 4.4. Although, the main resonant frequency at 2.40 GHz shows good agreement in both frequency and return loss, the measured bandwidth is significantly narrower than in the simulated case.

At around 5.8 GHz, the simulation did not indicate a sharp resonance, but the measured data show a shallow dip at this frequency, confirming partial energy coupling. Interestingly, the measured response reveals a strong and sharp resonance at 6.05 GHz with a return loss of –33.83 dB, which was not present in the same form in the simulation.

This discrepancy may be due to fabrication tolerances, connector effects or unmodeled losses in the substrate.

Table 4.4: *Comparison of Simulated and Measured Resonant Frequencies*

Mode	Simulated (GHz)	Measured (GHz)	Comment
1st Resonance	2.40 (–14.2 dB)	2.40 (–13.98 dB)	Narrower BW in measurement
2nd Resonance	6.2 (–25 dB)	6.05 (–33.83 dB)	Slightly shifted in real case

4.3 Design of Compact Multiband Fractal Monopole Antenna with Alumina Substrate

To evaluate the impact of a high permittivity substrate on antenna performance, the same Koch based multiband fractal antenna was resimulated using Alumina (Al_2O_3), a ceramic substrate with a relative permittivity of approximately $\varepsilon_r = 9.8$ and a very low loss tangent. The high dielectric loading of Alumina enabled a significant reduction in the overall antenna size, approximately 35% smaller than its FR-4 counterpart, while still maintaining resonant frequencies near 2.4 GHz and 5.8 GHz, which are widely used in ISM and Wi-Fi communication bands. Several parametric sweeps were performed to analyze how individual design variables influenced antenna behavior. Increasing the height of the feed line (h) shifted the resonant frequency downward and slightly improved impedance matching, although at the cost of a narrower bandwidth. A height of 20 mm was determined to provide an optimal balance between miniaturization and frequency stability. Feedline width (L_g) variations showed that the best performance was achieved at $L_g = 1.1$ mm, offering optimal impedance matching and minimal return loss near the target frequencies. Wider feedlines were found to excessively decrease input impedance and introduce undesirable shifts in resonance. Ground plane width (GRD) adjustments affected especially the higher frequency band (5.8 GHz), with narrower ground planes improving coupling but increasing back radiation and pattern asymmetry. These results demonstrate that the Alumina based antenna design, despite its fabrication complexity, offers sharper resonances and better size efficiency compared to FR-4, making it highly suitable for compact wireless applications operating in 2.4 GHz and 5.8 GHz bands.

Figures 4.13, 4.14 and 4.15 show the parametric simulation results based on the variations of variables h, L_g and GRD. According to these results, selected values of these variables for a balanced antenna are given in Table 4.5.

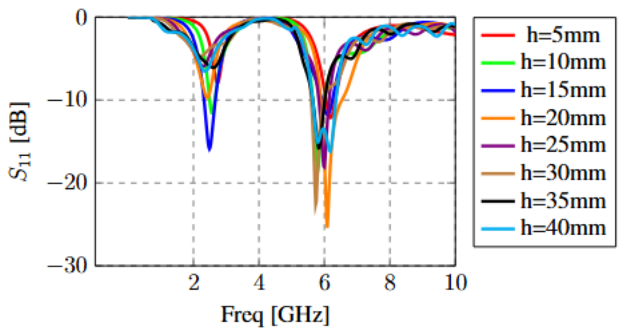

Figure 4.13: *Variation of S_{11} response with feedline height (h) directly affects resonance positions with Alumina*

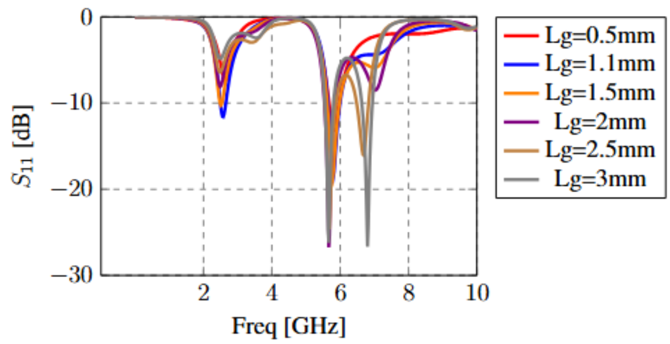

Figure 4.14: *Variation of S_{11} response with antenna feedline width (Lg) directly affects resonance positions with Alumina*

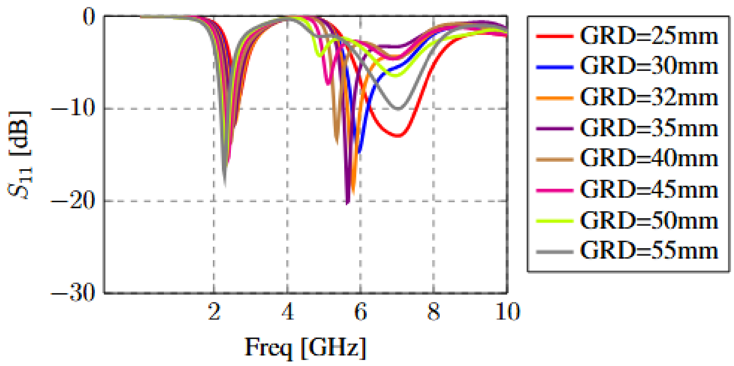

Figure 4.15: *Variation of S_{11} response with antenna ground plane (GRD) directly affects resonance positions with Alumina*

Table 4.5: *Designed antenna dimensions with Alumina*

Parameter	**Optimized Size (mm)**
L	13.00
W	6.00
GRD	32.00
h	10.00
Lg	1.10

Table 4.6 presents a side by side comparison of the optimized antenna dimensions for FR-4 and Alumina substrates. The results clearly show a significant reduction in overall antenna size when switching to Alumina, with the antenna length and width decreasing by over 35% and 65% respectively. This miniaturization is primarily enabled by Alumina's higher relative permittivity ($\varepsilon_r = 9.8$), which allows shorter electrical paths. In addition, feedline height and width were also reduced accordingly, contributing to more compact and efficient design suitable for modern wireless applications.

The comparative analysis of antenna dimensions in Table 4.6 highlights the substantial miniaturization achieved by employing Alumina instead of FR-4 as the substrate material. Due to its significantly higher relative permittivity, Alumina enables the realization of compact antenna structures without compromising the resonant frequency characteristics. The antenna length decreased from 21.00 mm to 13.00 mm and the width reduced from 18.93 mm to 6.00 mm, representing size reductions of approximately 38% and 68%, respectively. Additionally, the feedline and radiator height values were also lowered, which contributes not only to a smaller form factor but also to enhanced fabrication feasibility in dense and embedded wireless systems. These results confirm that substrate permittivity is a dominant factor in size constrained antenna design and Alumina provides an effective path toward compact high frequency applications.

Table 4.6: *Comparison of Optimized Antenna Dimensions for FR-4 and Alumina Substrates*

Parameter	**FR-4 (mm)**	**Alumina (mm)**
L (Radiator Length)	21.00	13.00
W (Radiator Width)	18.93	6.00
GRD (Ground Width)	45.00	32.00
h (Feedline Height)	20.00	10.00
L_g (Feedline Width)	3.00	1.10

The final S_{11} graph of the fractal antenna created with the determined parameters and alumina substrate is shown in Figure 4.16. In Figures 4.17 and 4.18, the E and H plane radiation patterns corresponding to the frequencies of 2.4 GHz and 5.8 GHz, are shown.

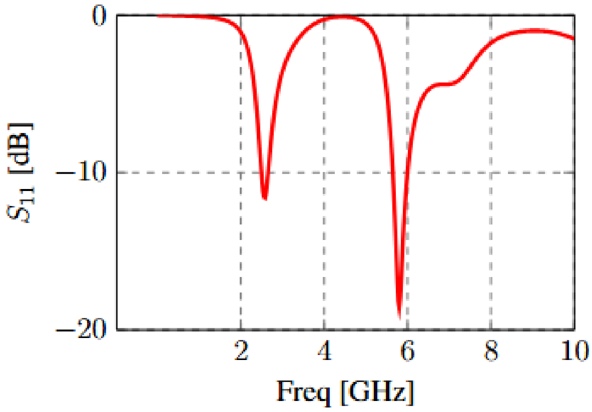

Figure 4.16: *The S_{11} responses of the third iteration Koch fractal monopole antenna with Alumina*

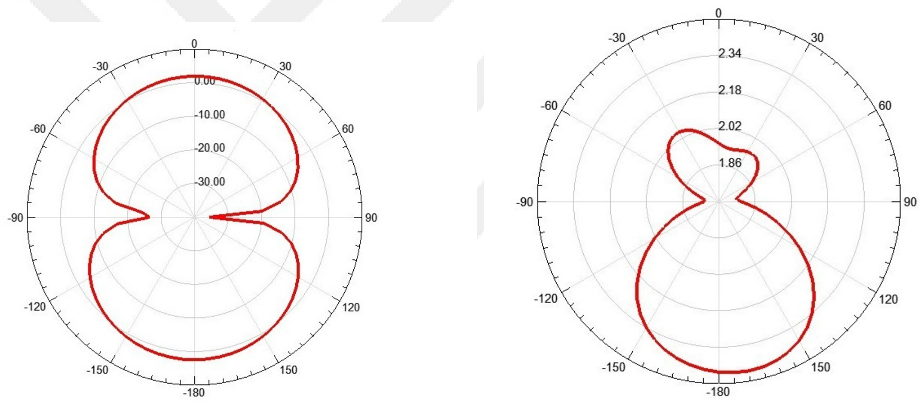

Figure 4.17: *2D radiation patterns at 2.4 GHz. Left: E-plane, Right: H-plane.*

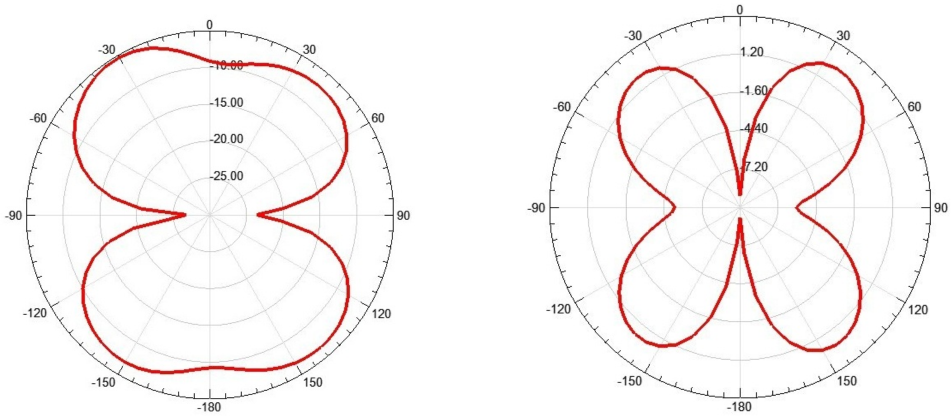

Figure 4.18: *2D radiation patterns at 5.8 GHz. Left: E-plane, Right: H-plane.*

The far field 3D radiation patterns, presented in Figure 4.19, further validate the multiband behavior and directional nature at higher frequencies. The gain at 2.4 GHz was measured to be 2.46 dBi and at 5.8 GHz to be 4.4 dBi, which are satisfactory for compact antenna designs with fractal geometries.

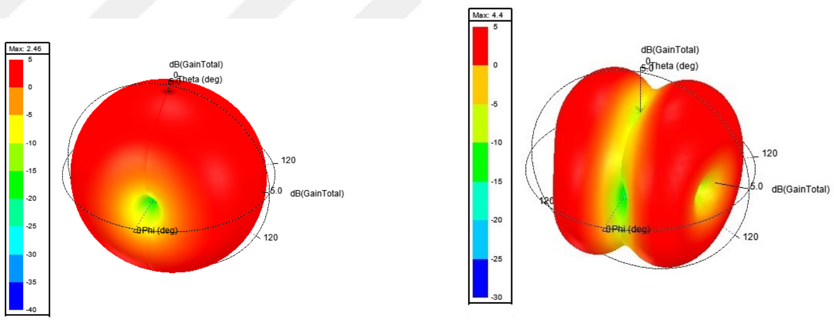

Figure 4.19: *3D radiation patterns of the proposed antenna at 2.4 GHz (left) and 5.8 GHz (right).*

Extending the substrate dimensions while keeping the conductor geometry unchanged can still influence the antenna's performance, as it alters the effective dielectric constant surrounding the radiating element. This modification affects the distribution of the electromagnetic fields, leading to a shift in the resonant frequency and changes in the input impedance. Furthermore, an enlarged substrate area increases the portion of the electromagnetic energy stored within the dielectric material, which may result in higher dielectric losses and consequently lower radiation efficiency. Therefore, the substrate size must be carefully optimized to provide sufficient mechanical support without degrading the antenna's electrical performance.

The Figure 4.20 shows the antennas with a 10 mm top extended and 5 mm extended on each side. The simulation results obtained for this antenna are presented in the Figure 4.21. The results show the shift in resonant frequency and changes in return loss due to substrate extension.

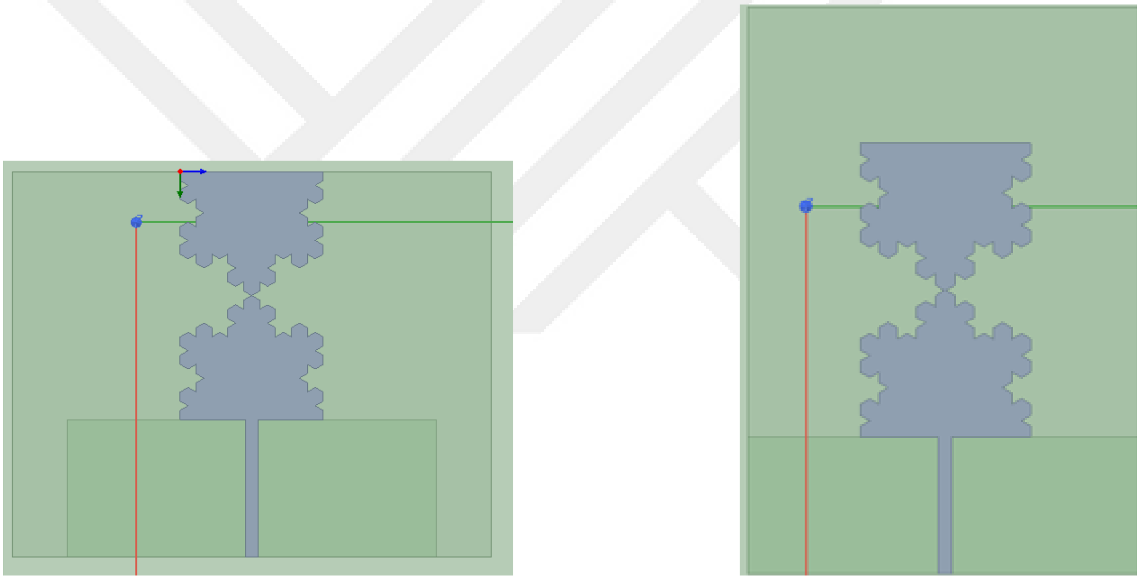

(a) Side extended substrate (b) Top extended substrate

Figure 4.20: *Extended Antennas*

To investigate the effects of substrate thickness on antenna performance, the proposed antenna was simulated using Alumina substrates with thicknesses of 0.635 mm and 1 mm. The substrate thickness directly affects the effective dielectric constant, which in turn modifies the input impedance, resonant frequency and bandwidth of the antenna.

Figure 4.22 shows the simulated S_{11} responses for both thicknesses. It is observed that increasing the substrate thickness slightly shifts the resonant frequency downward

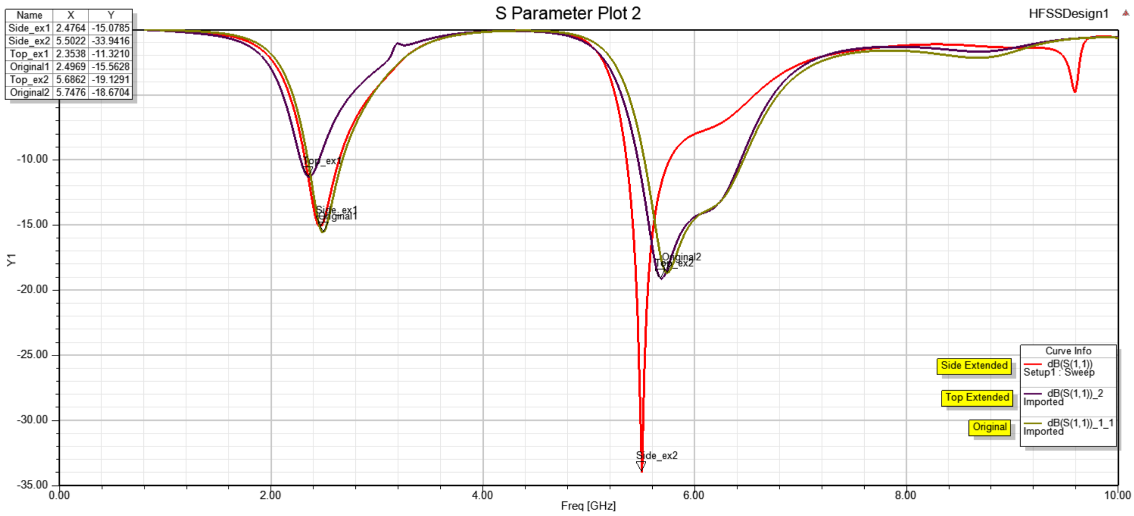

Figure 4.21: *Comparison of extended antennas*

and improves impedance matching at the lower band while the higher frequency bands show minor changes. The thicker substrate also results in a slightly wider bandwidth due to the increased effective capacitance between the radiating element and ground plane. However, very thick substrates may lead to undesired surface wave excitation and slight degradation in radiation efficiency, so an optimal thickness must be chosen based on the trade off between miniaturization and electrical performance.

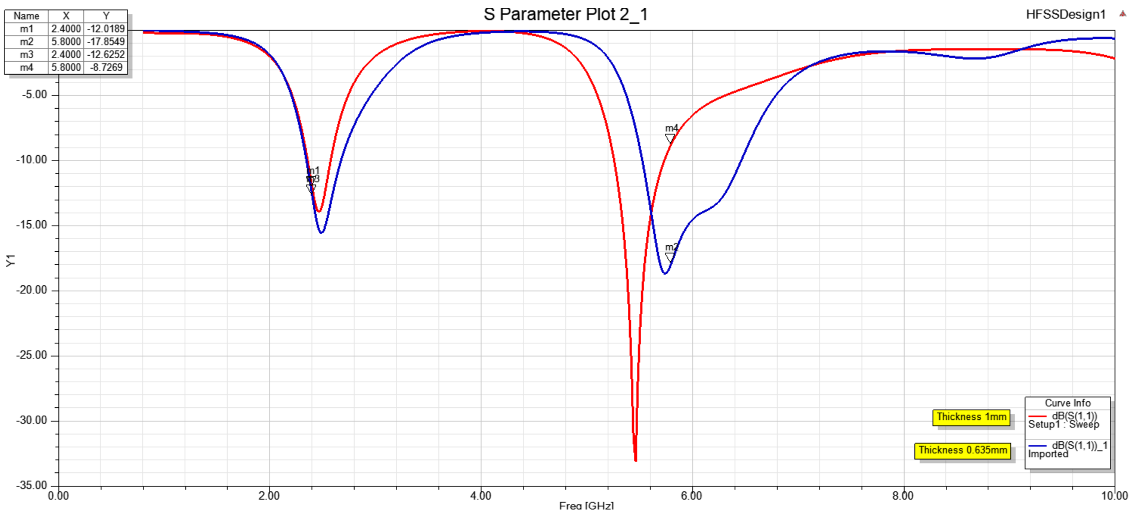

Figure 4.22: *Simulated S_{11} responses of the proposed Alumina RFID antenna with substrate thicknesses of 0.635 mm and 1 mm.*

4.4 Design of Multiband Fractal Antenna for RFID Using FR-4 Substrate

In this section, an RFID antenna is developed by scaling up the dimensions of the previously optimized third iteration of the Koch fractal monopole antenna. The primary objective of this design is to achieve resonance near the UHF RFID frequency band, specifically around 866 MHz.

To accommodate the lower frequency requirement with FR-4 substrate, the physical dimensions of the antenna were significantly increased while maintaining the fractal structure on the radiating edges to ensure compactness and multiband behavior. The optimized dimensions of the proposed RFID antenna are summarized in Table 4.7.

Table 4.7: *Design Parameters of the Proposed RFID Antenna*

Parameter	Antenna Size [mm]
L	67.2
W	64.3
h	66.2
GRD	144
Lg	6

The antenna was modeled and simulated using ANSYS HFSS, a full wave 3D electromagnetic solver. Figure 4.23 presents the simulated return loss S_{11}, demonstrating that the antenna supports multiple resonant frequencies at 866 MHz (targeted for UHF RFID), 2.4 GHz, 4.2 GHz, 5.0 GHz, 5.8 GHz, 6.7 GHz and 7.3 GHz.

The radiation characteristics were further analyzed at all resonant frequencies. Figures 4.24 through 4.30 show the 2D radiation patterns in both the E-plane and H-plane at each resonant frequency. Furthermore, the 3D far field radiation patterns are illustrated in Figure 4.31, which confirms the omnidirectional behavior in the lower bands and the more directive characteristics in the higher bands.

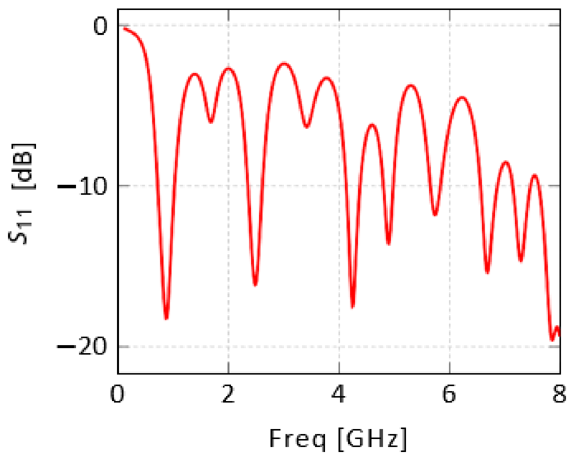

Figure 4.23: *Simulated S_{11} of the proposed RFID antenna showing multiband operation.*

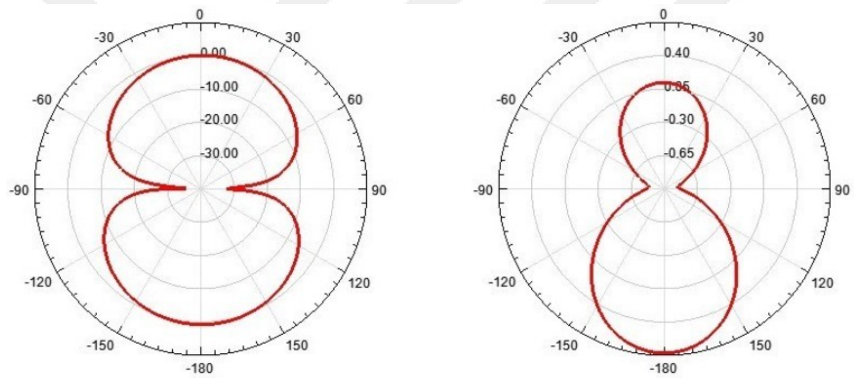

Figure 4.24: *2D Radiation patterns at 866 MHz: Left: E-plane, Right H-plane.*

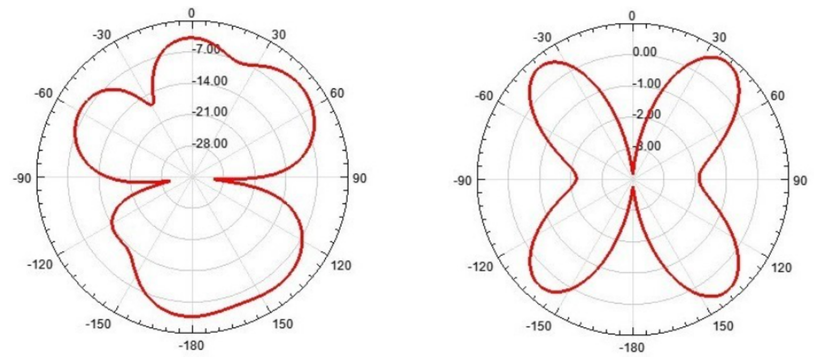

Figure 4.25: *2D Radiation patterns at 2.4 GHz: Left: E-plane, Right H-plane.*

4.4.1 Measured Results

To experimentally verify the simulation results at 866 MHz frequency, the proposed fractal antenna was fabricated on a FR-4 substrate using standard PCB fabrication

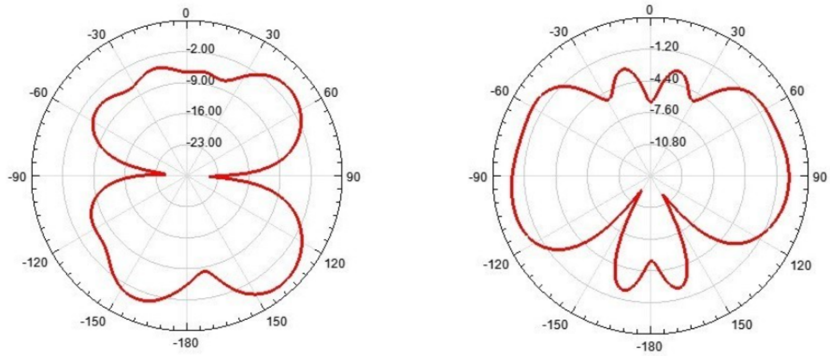

Figure 4.26: *2D Radiation patterns at 4.2 GHz: Left: E-plane, Right H-plane.*

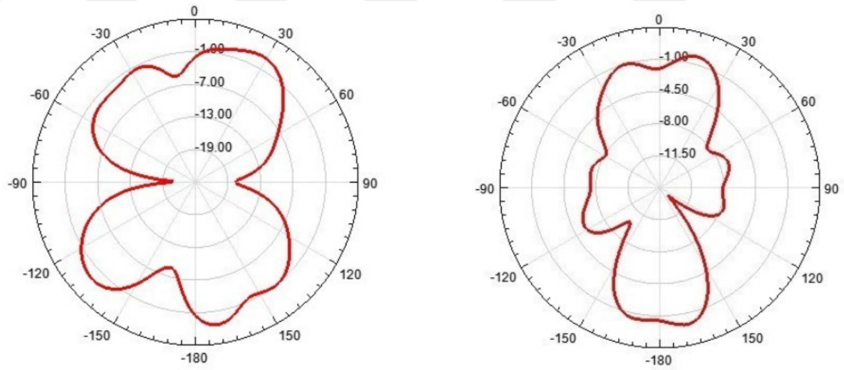

Figure 4.27: *2D Radiation patterns at 5 GHz: Left: E-plane, Right H-plane.*

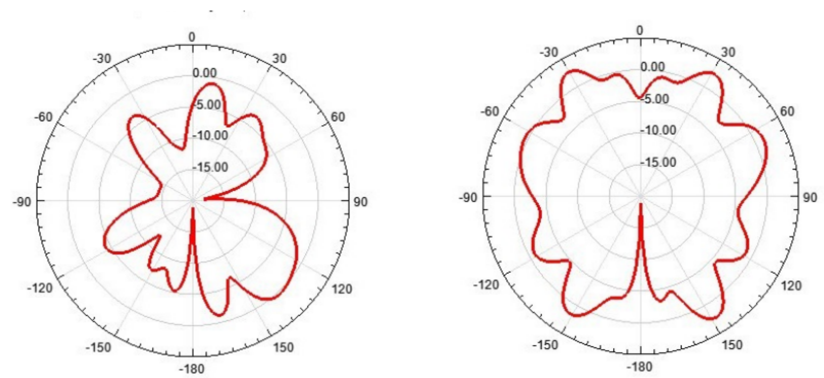

Figure 4.28: *2D Radiation patterns at 5.8 GHz: Left: E-plane, Right H-plane.*

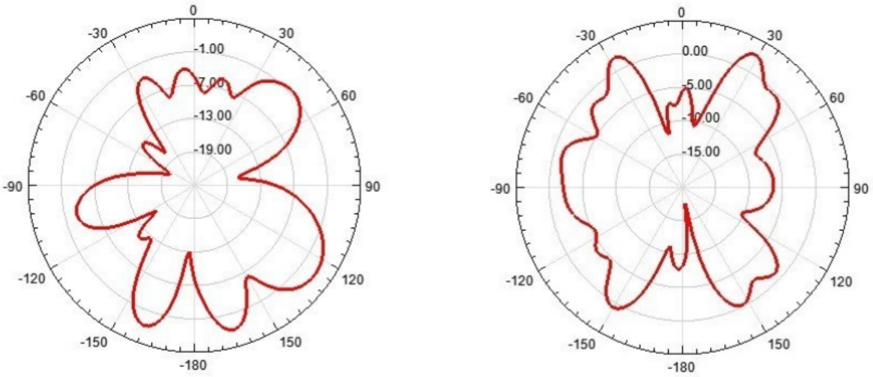

Figure 4.29: *2D Radiation patterns at 6.7 GHz: Left: E-plane, Right H-plane.*

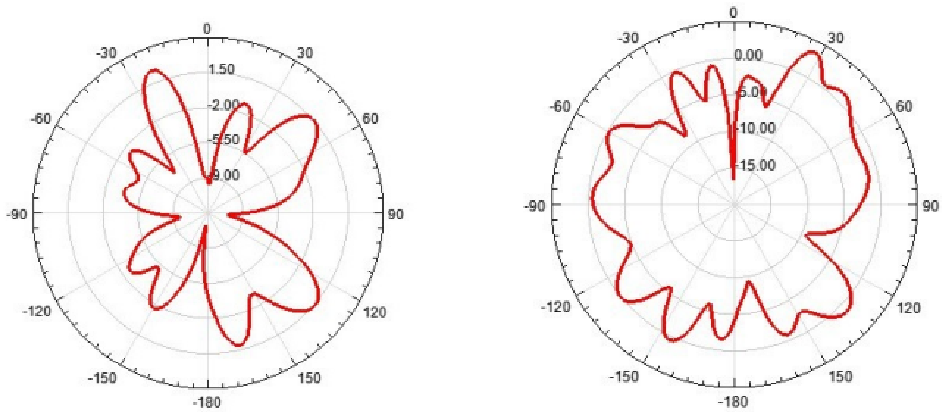

Figure 4.30: *2D Radiation patterns at 7.3 GHz: Left: E-plane, Right H-plane.*

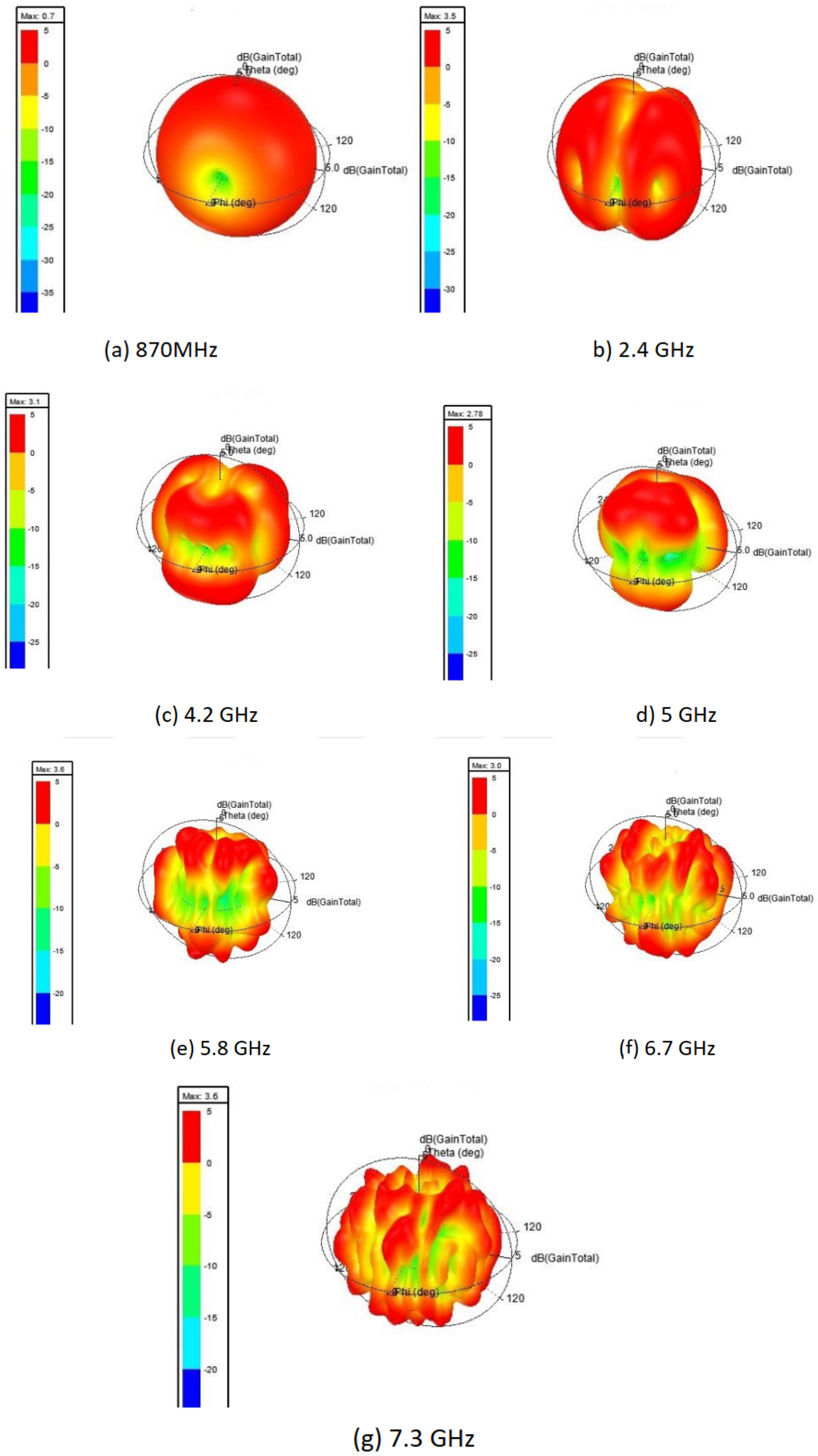

Figure 4.31: *3D far field radiation patterns of the proposed antenna at all resonant frequencies.*

techniques. Measurements were performed using a Keysight PNA-X Vector Network Analyzer (Model N5242B) after performing a 2 port calibration using the Keysight N4691B electronic calibration module as shown in Figure 4.10. The frequency scan was configured from 10 MHz to 10 GHz with a power level of –5 dBm and 451 number of points. In Figure 4.32, the fabricated antenna can also be seen while taking the measurement.

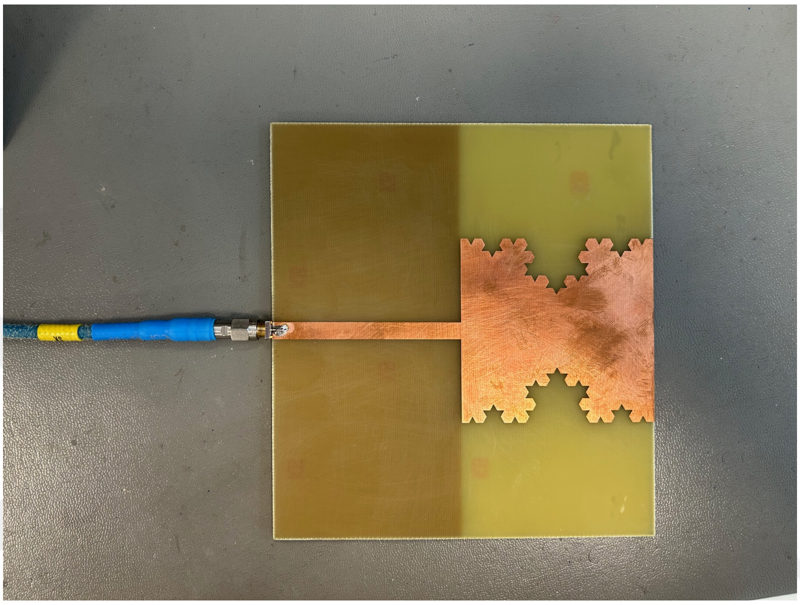

Figure 4.32: *Photograph of the RFID included fabricated antenna*

Obtained return loss S_{11} graph of the fabricated antenna from experimental test setup is shown in Figure 4.33. These results show strong agreement with the simulation results presented earlier. They are very similar to the simulation results at the desired frequencies, 866 MHz, 2.4 GHz and 5.8 GHz and they are below the –10 dB value required for a good antenna performance. This is an indication that the simulation results are correct and that calibration is done correctly. It has been confirmed that multiband, small size and efficient antennas can be obtained at these frequencies by using the Koch fractal structure. The S_{11} results obtained from the network analyzer are summarized in Table 4.8, indicating the desired frequencies.

To evaluate the performance of the proposed antenna, a comparative analysis with

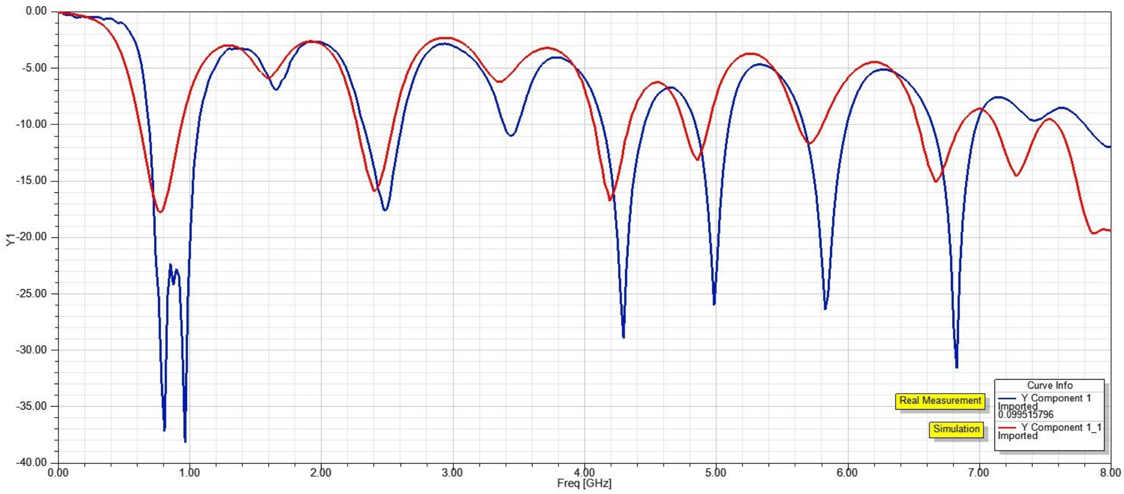

Figure 4.33: *The S_{11} responses of the fabricated and simulated RFID antennas*

Table 4.8: *Measured S_{11} values*

Frequency (GHz)	Return Loss (dB)
0.866	–21.37
2.40	–13.83
5.80	–21.90

previously published RFID/multiband antennas is presented in Table 4.9. The relatively large wavelength associated with the 866 MHz band makes the integration of this frequency challenging in multiband antenna designs. Consequently, few examples are found in the literature; nevertheless, the available design demonstrates a significant reduction in overall dimensions.

Table 4.9: *Comparison of Proposed Antenna with Published Literature*

Reference	Size [mm^3]	Resonant Frequencies (GHz)	S11 (dB)
Ref [32]	290×290×1.6	0.868/ 2.4	-11/ -20
Proposed	133.4×144.4×1.6	0.866/ 2.4/ 4.2/ 5.8/ 6.7	-21/ -13/ -28/ -21/ -31

In order to minimize reflections caused by surrounding objects during the return loss measurement of the fabricated antenna, the antenna should ideally be placed at a distance of one wavelength from all nearby objects. Nearby surfaces interact with the near field of the antenna. This can shift the resonant frequency and distort the S_{11} values.

To analyze this effect, two measurements were taken using the fabricated antenna. In the first measurement, the antenna was fixed at a height of one wavelength above the table. The second measurement was taken while the antenna was placed directly on the table. These two results can be observed together in Figure 4.34, where the marked trace corresponds to the measurement taken directly on the table. As a result, it can be observed that the frequencies are slightly shifted and the S_{11} values are increased.

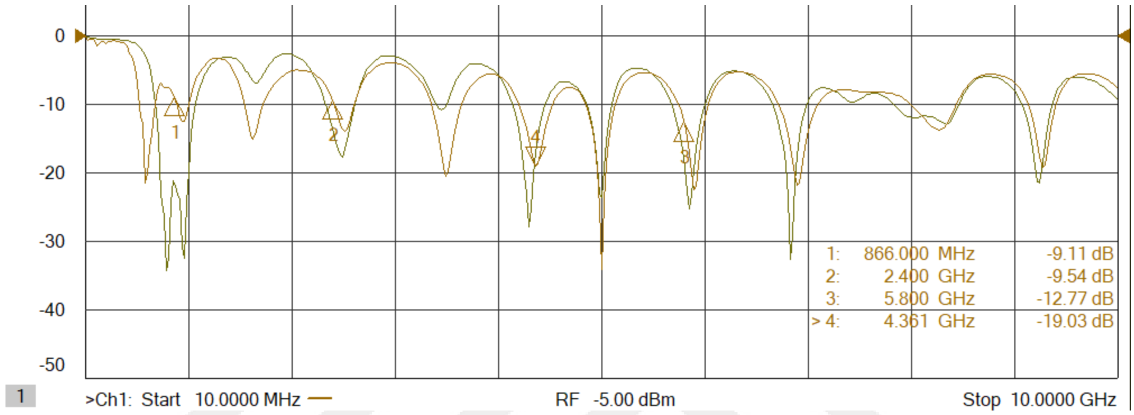

Figure 4.34: *Comparison of the antenna height*

4.5 Design of Multiband Fractal Antenna for RFID Using Alumina Substrate

In the design of RFID antennas using an Alumina substrate, a natural size reduction was achieved due to its high relative permittivity ($\varepsilon_r = 9.8$), compared to the conventional FR-4 material. However, in order to maintain resonance at 866 MHz, the effective electrical length of the antenna had to be preserved. To accomplish this, slots were introduced into the antenna structure, effectively increasing the current path without enlarging the physical dimensions. The use of slots not only contributed to miniaturization, but also improved impedance matching, resulting in a lower reflection coefficient S_{11}. This slot assisted design approach provided a compact antenna footprint, approximately 30–40% smaller than the FR-4 based version, while simultaneously delivering enhanced electrical performance. In Figure 4.35, the antenna structure obtained with alumina substrate, the mentioned slots and their dimensions are shown. In Table 4.10, all variable values are given.

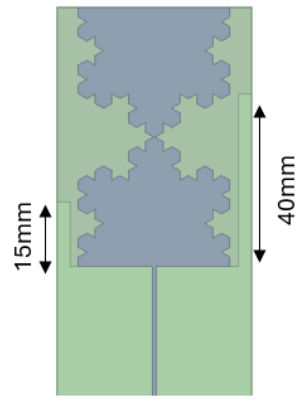

Figure 4.35: *Proposed RFID Antenna with Alumina Substrate*

Table 4.10: *Optimized Dimensions of the Proposed RFID Antenna with Alumina Substrate*

Parameter	Antenna Size [mm]
L	60
W	35
h	30
GRD	45
Lg	1

Simulation was also performed for the antenna designed with alumina substrate. The simulation result of S_{11} response is shown in Figure 4.36. When the simulation results are compared with the FR-4 antenna, it is seen that although the dimensions of the Alumina antenna are smaller, S_{11} values at frequencies of 2.4 GHz and 5.8 GHz are better than the FR-4 antenna. At the frequency of 866 MHz, S_{11} value is observed to be approximately 2 dB worse than the FR-4 antenna, but the requirement is still met with –15 dB.

In addition to simulations of other antenna designs, Figure 4.37 shows the current

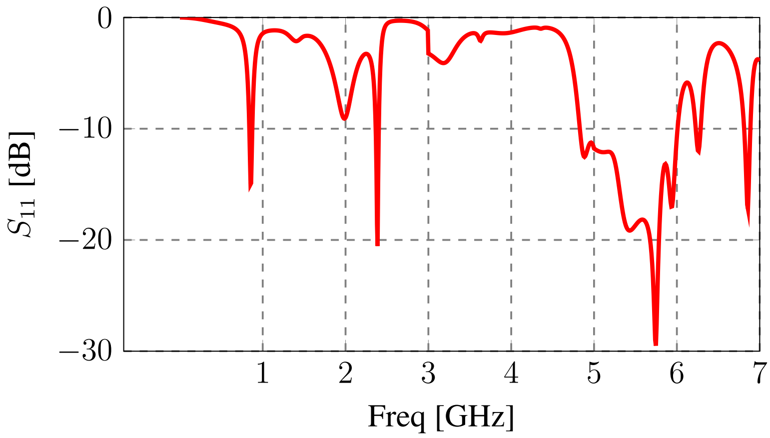

Figure 4.36: *The S_{11} responses of the third iteration Koch fractal monopole antenna with Alumina*

density simulation and effect of the opened slots to reduce the reflection at the frequency of 866 MHz to the desired level. In this way, the reflection value at the frequency of 866 MHz also meets the antenna requirements.

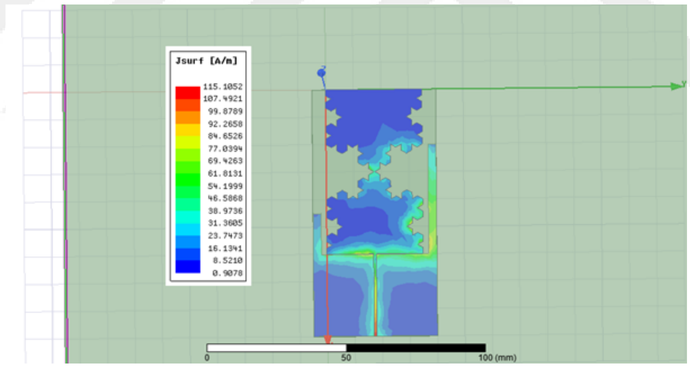

Figure 4.37: *Current density of proposed alumina antenna*

The radiation characteristics were further analyzed at all desired frequencies, 866 MHz, 2.4 GHz, 5.8 GHz. Figures 4.38 through 4.40 show the 2D radiation patterns in both the E-plane and H-plane at these frequencies. Furthermore, 3D far field radiation patterns are illustrated in Figure 4.41, which confirms the omnidirectional behavior in the lower bands and the more directive characteristics in the higher bands. When these results are compared with FR-4 material, it can be said that similar results are obtained with alumina antenna although its dimensions are smaller.

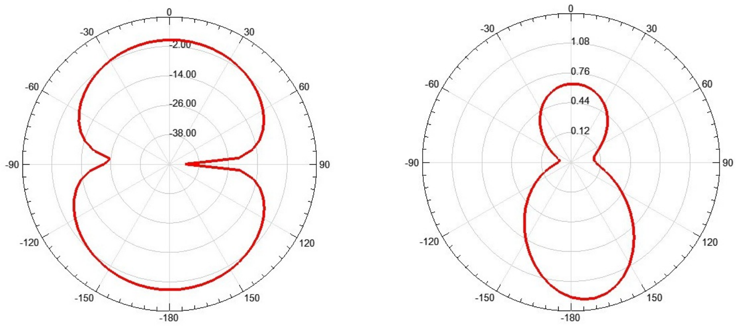

Figure 4.38: *2D Radiation patterns at 866 MHz: Left: E-plane, Right H-plane.*

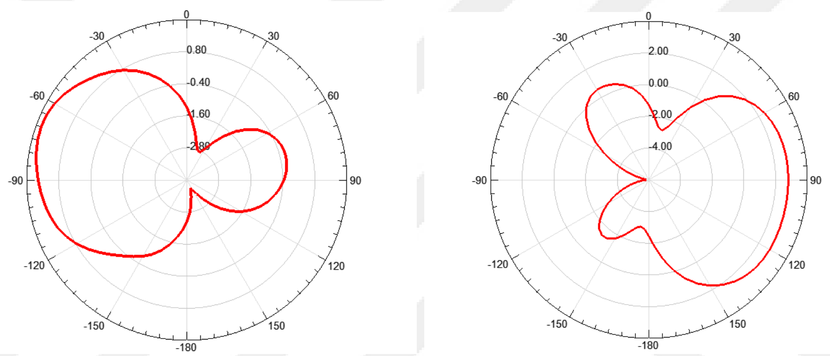

Figure 4.39: *2D Radiation patterns at 2.4 GHz: Left: E-plane, Right H-plane.*

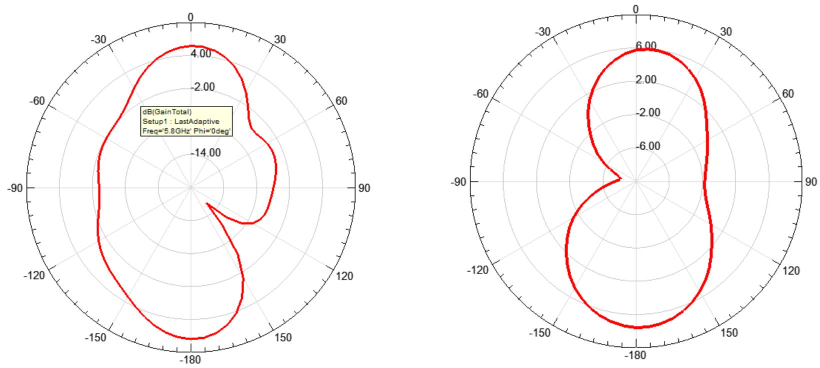

Figure 4.40: *2D Radiation patterns at 5.8 GHz: Left: E-plane, Right H-plane.*

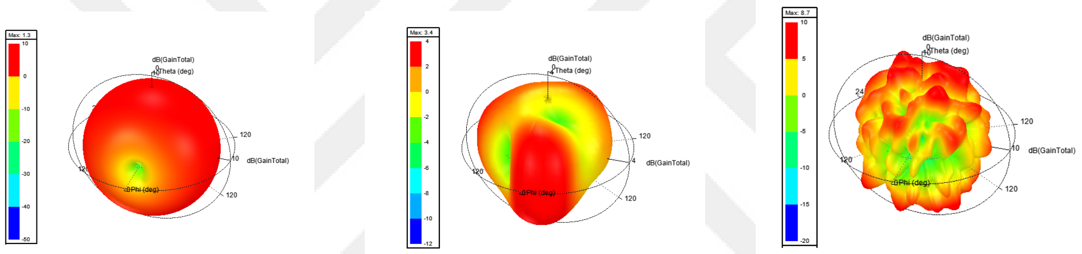

(a) 866 MHz **(b)** 2.4 GHz **(c)** 5.8 GHz

Figure 4.41: *3D far field radiation patterns of the proposed antenna at its resonant frequencies.*

5. CONCLUSIONS

This thesis addresses the design, optimization, and performance evaluation of a multiband fractal antenna by examining the iterations of the Koch curve, specifically tailored for RFID and wireless communication applications. The primary objective is to investigate the effect of Koch fractal iterations on the performance of multiband antennas and analyze their applicability in RFID and wireless communication systems. Additionally, without altering the geometric configuration of the antenna structure, the study analyzes how different substrate materials with varying dielectric properties, such as FR-4 and Alumina (Al_2O_3), influence key antenna characteristics including size, bandwidth, resonant frequencies, gain, and radiation patterns.

The antennas were modeled and simulated using ANSYS HFSS, a widely accepted high frequency electromagnetic simulation tool. A systematic parametric analysis was performed to evaluate the impact of critical design parameters such as patch height, feedline width, and ground plane dimensions. These variables were optimized to improve impedance matching, enhance radiation efficiency, and achieve stable multiband behavior. The use of the Koch curve geometry enabled the antenna to achieve multiband operation, thanks to the inherent properties of fractals such as self similarity, scale invariance, and space filling behavior.

Simulation results revealed that both antennas on FR-4 and Alumina substrates, exhibited resonances around 866 MHz, 2.4 GHz, and 5.8 GHz, which are key frequencies for RFID, Wi-Fi, and ISM applications, respectively. The antenna constructed on the Alumina substrate demonstrated superior miniaturization capabilities due to its high relative permittivity ($\varepsilon_r \approx 9.8$) and low loss tangent, allowing for sharper resonance and improved energy confinement. In contrast, the FR-4 based design, with a lower permittivity ($\varepsilon_r \approx 4.4$), offered wider bandwidth performance but required a larger physical footprint to maintain acceptable resonance characteristics.

In terms of return loss S_{11}, VSWR, and bandwidth, both antennas met the performance thresholds ($S_{11} < -10$ dB) required for efficient operation. However, the tradeoff between size and bandwidth became evident. While the Alumina based antenna stood out in terms of compactness and frequency selectivity, the FR-4 based antenna delivered better performance across wider frequency ranges. Therefore, if there is a space constraint and more precise operation is desired, the Alumina based antenna will clearly offer better performance. On the other hand, if there is no space limitation, and working with wider bandwidths while considering tolerances is acceptable, and especially if a PCB made of FR-4 is already in use, the FR-4 based antenna would be more suitable, as it can also be implemented on board.

Radiation pattern analyses, in both 2D and 3D, confirmed that the proposed antenna maintained good directional behavior and consistent gain across its resonant frequencies. The fractal geometry contributed not only to miniaturization but also to the establishment of multiple resonant paths, thus supporting stable multiband operation. Furthermore, the radiation efficiency and gain results were within acceptable ranges for practical RFID reader and tag implementations, as well as short to medium range wireless communication systems.

From a broader perspective, this thesis contributes to the advancement of antenna engineering based on fractal geometry. It also offers a different perspective for overcoming certain design constraints by taking substrate effects into account. The study demonstrates that careful selection of substrate material can significantly influence antenna performance without requiring any changes to geometric design of the antenna. The findings highlight the importance of both antenna geometry and substrate properties in achieving design tradeoffs among miniaturization, bandwidth, and fabrication cost.

In conclusion, the proposed Koch based fractal antenna structure offers a promising solution for compact and efficient multiband antennas used in modern wireless applications. The comparison between FR-4 and Alumina substrates provides valuable insight for antenna designers seeking to tailor antenna performance to specific application needs. Future work may include the fabrication and measurement of the Alumina based design, exploration of additional high permittivity substrates, or integration of reconfigurable elements for dynamic frequency tuning. The results of this study provide a solid foundation for the development of next generation RFID and wireless antennas in compact and high performance environments.

In the future, it is evident that by developing a different fractal geometry, selecting an alternative substrate material or implementing modifications such as slots on the Alumina based antenna to enable operation at RFID frequencies, it would be possible to achieve operation at different frequencies. Perhaps these studies could be adapted using today's popular technology, artificial intelligence, to improve the parametric simulation results achieved in this study at the same frequencies.

REFERENCES

[1] C. A. Balanis, *Antenna Theory: Analysis and Design*. John Wiley & Sons, 4 ed., 2016.

[2] D. M. Pozar, *Microwave Engineering*. John Wiley & Sons, 4 ed., 2012.

[3] W. L. Stutzman and G. A. Thiele, *Antenna Theory and Design*. John Wiley & Sons, 3rd ed., 2012.

[4] D. H. Werner and R. Mittra, "Fractal antenna engineering: The theory and design of fractal antenna arrays," *IEEE Antennas and Propagation Magazine*, vol. 41, no. 5, pp. 37–58, 1999.

[5] C. Puente, J. Romeu, R. Pous, and A. Cardama, "Fractal multiband antenna based on the sierpinski gasket," *Electronics Letters*, vol. 32, no. 1, pp. 1–2, 1996.

[6] K. Finkenzeller, *RFID Handbook: Fundamentals and Applications in Contactless Smart Cards, Radio Frequency Identification and Near-Field Communication*. John Wiley & Sons, 2010.

[7] S. Wang, D. Kim, and J. Choi, "Design of compact rfid tag antennas using fractal geometries," *IEEE Antennas and Wireless Propagation Letters*, vol. 12, pp. 1192–1195, 2013.

[8] E. Liew, M. Malaysia, S. Malaysia, T.-A. Okubo, T. Sudo, T. Hosoi, H. Tsuyoshi, and F. Kuwako, "Signal transmission loss due to copper surface roughness in high-frequency region," *Journal of Microwaves, Optoelectronics and Electromagnetic Applications*, 01 2014.

[9] S. J. Penn, N. M. Alford, A. Templeton, X. Wang, M. Xu, M. Reece, and K. Schrapel, "Effect of porosity and grain size on the microwave dielectric properties of sintered alumina," *Journal of the American Ceramic Society*, vol. 80, no. 7, pp. 1885–1888, 1997.

[10] J. P. Gianvittorio and Y. Rahmat-Samii, "Fractal antennas: A novel antenna miniaturization technique, and applications," *IEEE Antennas and Propagation Magazine*, vol. 44, no. 1, pp. 20–36, 2002.

[11] H. Visser and R. Vullers, "Rf energy harvesting and transport for wireless sensor network applications: Principles and requirements," *Proceedings of the IEEE*, vol. 101, p. 1410, 06 2013.

[12] N. Cohen, "Fractal antenna applications in wireless telecommunications," in *Professional Program Proceedings: Electronics Industries Forum of New England*, pp. 43–49, IEEE, 1997.

[13] D. Werner and S. Ganguly, "An overview of fractal antenna engineering," *Antennas and Propagation Magazine*, vol. 45, pp. 38–57, 2003.

[14] I. J. Bahl and P. Bhartia, "A compact radio frequency identification tag antenna using fractal geometry," *Microwave Journal*, vol. 46, no. 11, pp. 76–84, 2003.

[15] E. Brown, *Wireless Communication Systems: Principles and Practice*. TechPress, 2021.

[16] J. L. Volakis and K. Sertel, "A review of substrate effects on printed antennas: Performance enhancement using artificial materials and substrates," *IEEE Antennas and Propagation Magazine*, vol. 52, no. 5, pp. 72–79, 2010.

[17] R. Kumar and A. Singh, "Substrate effects on the performance of microstrip patch antennas: A review," *International Journal of Microwave and Wireless Technologies*, vol. 9, no. 4, pp. 821–829, 2017.

[18] N. Sharma and J. Singh, "Effect of dielectric substrate on microstrip patch antenna performance," *International Journal of Antennas and Propagation*, vol. 2019, pp. 1–9, 2019.

[19] T. S. Bird, "Definition and misuse of return loss [report of the transactions editor-in-chief]," *IEEE Antennas and Propagation Magazine*, vol. 51, no. 2, pp. 166–167, 2009.

[20] J. D. Kraus and R. J. Marhefka, *Antennas for All Applications*. McGraw-Hill Education, 3 ed., 2002.

[21] R. F. Harrington, "Effect of antenna size on gain, bandwidth, and efficiency," *Journal of Research of the National Bureau of Standards*, vol. 64D, no. 1, pp. 1–12, 1960.

[22] B. A. P. Nel, A. K. Skrivervik, and M. Gustafsson, "Radiation efficiency and gain bounds for microstrip patch antennas," *arXiv preprint arXiv:2403.18844*, 2024.

[23] M. Shahpari and D. V. Thiel, "Fundamental limitations for antenna radiation efficiency," *arXiv preprint arXiv:1609.01761*, 2016.

[24] H. Rajabloo, V. A. Kooshki, and H. Oraizi, "Compact microstrip fractal koch slot antenna with elc coupling load for triple band application," *AEU - International Journal of Electronics and Communications*, vol. 73, pp. 144–149, 2017.

[25] T. Ali, M. S. Aw, and R. Biradar, "A fractal quad-band antenna loaded with l-shaped slot and metamaterial for wireless applications," *International Journal of Microwave and Wireless Technologies*, pp. 1–9, 2018.

[26] B. B. Mandelbrot, *The Fractal Geometry of Nature*. W. H. Freeman and Company, 1982.

[27] N. Cohen, “Fractal antennas: A review,” *Progress In Electromagnetics Research*, vol. 51, pp. 1–22, 1999.

[28] S. A. E. Team, “Romanesco broccoli displays fractal-esque self-similar structure,” *Scientific American*, 2009.

[29] “Captured lightning: fractal-like lichtenberg figures frozen in acrylic blocks by bert hickman.” Online picture gallery, *The Telegraph*, Dec. 2009. Credit: Mike Walker / Rex Features.

[30] Mathigon, “Fractal fern leaf – fractals course introduction.” `https://mathigon.org/course/fractals/introduction`, 2023. July 2025.

[31] Wikipedia contributors, “Fractal dimension of koch snowflake.” `https://en.wikipedia.org/wiki/Fractal_dimension`. July 2025.

[32] M. Rusu, M. Hirvonen, H. Rahimi, P. Enoksson, C. Rusu, N. Pesonen, O. Vermesan, and H. Rustad, “Minkowski fractal microstrip antenna for rfid tags,” in *2008 38th European Microwave Conference*, pp. 666–669, 2008.

[33] M. F. Barnsley, *FractalsEverywhere*. Boston,MA,USA: Academic Press, 1988.

[34] W. J. Krzysztofik, “Fractal geometry in electromagnetics applications,” *Microwaves, Antennas & Propagation*, vol. 19, no. 2, pp. 14–25, 2013. Extended version of TELSIKS 2013 paper.

[35] A. Salih and M. S. Sharawi, “A dual-band highly miniaturized patch antenna,” *IEEE Antennas and Wireless Propagation Letters*, vol. 15, pp. 1783–1786, 2016.

[36] M. T. Yassen, M. R. Hussan, H. A. Hammas, A. J. Salim, and J. K. Ali, “Design of compact dual-band fractal monopole antenna with virtually extended ground plane,” *Advanced Electromagnetics*, vol. 7, no. 4, 2018.

[37] Agilent Technologies, “Advanced techniques for network analyzer calibration.” `https://anlage.umd.edu/Agilent_Advanced_VNA_calibration.pdf`, 2004. July 2025.